Article

Current Biology

Mitochondria transported by Kinesin-3 prevent localized calcium spiking to inhibit caspase-dependent specialized cell death

Graphical abstract

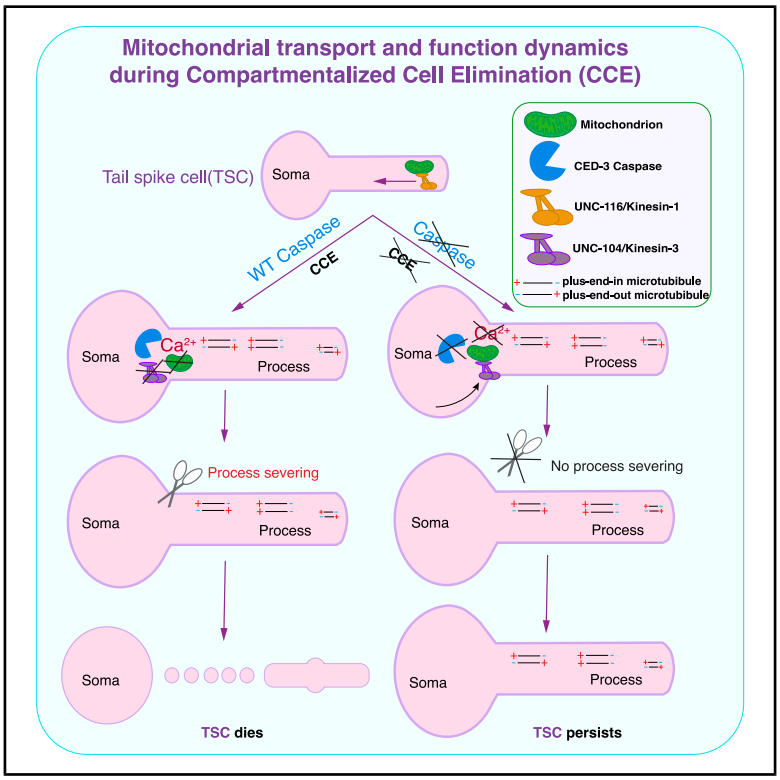

Highlights

- Mitochondrial transport by opposing kinesins directs specialized cell death
- Kinesin-1 removes mitochondria via atypical soma-directed transport
- Mitochondria are locally cytoprotective via MCU uniporter-dependent Ca^{2+} uptake
- Caspase locally inhibits the non-canonical mitochondrial transport role of Kinesin-3

Authors

Rashna Sharmin, Aladin Elkhalil, Sara Pena, ..., Mark W. Pellegrino, Shai Shaham, Piya Ghose

Correspondence

piya.ghose@uta.edu

In brief

Sharmin et al. define atypical roles for two kinesin motors in the transport of cytoprotective mitochondria during polarized cell death. Kinesin-1 ensures region-specific removal of mitochondria. Mitochondria can take up Ca^{2+} at the death initiation site and are transported there as non-canonical cargo of Kinesin-3, inhibited by local caspase.

Sharmin et al., 2025, Current Biology *35*, 4932–4945
October 20, 2025 Published by Elsevier Inc.
https://doi.org/10.1016/j.cub.2025.08.065

CellPress
OPEN ACCESS

Current Biology

Article

Mitochondria transported by Kinesin-3 prevent localized calcium spiking to inhibit caspase-dependent specialized cell death

Rashna Sharmin,[1] Aladin Elkhalil,[1] Sara Pena,[2] Pranya Gaddipati,[1] Ginger Clark,[1] Pavak K. Shah,[3] Mark W. Pellegrino,[1] Shai Shaham,[2] and Piya Ghose[1,4,*]

[1]The University of Texas at Arlington, Department of Biology, 501 S. Nedderman Dr., Arlington, TX 760109, USA
[2]The Rockefeller University, Laboratory of Developmental Genetics, 1230 York Ave., New York, NY 10065, USA
[3]The University of California, Los Angeles, Department of Molecular, Cell and Developmental Biology, 610 Charles E Young Dr., Los Angeles, CA 90095, USA
[4]Lead contact
*Correspondence: piya.ghose@uta.edu
https://doi.org/10.1016/j.cub.2025.08.065

SUMMARY

Polarized cells (such as neurons) have distinct compartments with differing functions, subcellular architecture, and microenvironments. Like many cell types, they are subject to programmed elimination as a part of normal development and homeostasis. We investigated the mechanism of specialized cell elimination by studying the embryonic cell death program, compartmentalized cell elimination (CCE), in the scaffolding tail-spike epithelial cell (TSC) of *C. elegans*. CCE, also seen in Cephalic male (CEM) sensory neurons, is stereotyped and ordered, with distinct programs eliminating each cell compartment—the soma and two segments of the single process, the latter resembling neurite pruning. Here, we report the atypical, compartment-specific roles of two kinesins in mitochondrial transport to regulate CCE. We show that UNC-116/Kinesin-1 is required to transport mitochondria out of the TSC process and that its absence results in distal mitochondrial retention and process persistence. We describe UNC-104/Kinesin-3 in the non-canonical role of mitochondrial transport that is negatively regulated by CED-3/caspase. We identify a degenerative hub of the TSC at the junction of the cell soma and process, characterized by local CED-3/caspase activity, Ca^{2+} increase, and membrane severing. In the absence of CED-3/caspase, early morphological hallmarks of CCE are seen; however, UNC-104/Kinesin-3 is permitted to carry mitochondria that take up local Ca^{2+}, leading to the reversal of CCE and cell recovery. Our study, by highlighting the involvement of region-specific Ca^{2+} signaling and caspase activity, the different contributions of mitochondria to cytoprotection, and the atypical roles of kinesin motors, sheds light on the molecular machinery of specialized cell elimination, with implications for cellular resilience.

INTRODUCTION

Programmed cell death is a vital feature of normal development and homeostasis.[1] For instance, the programmed elimination of supernumerary neurons in the early brain is a critical facet of neurodevelopment.[2–6] Specialized cells such as neurons present an especially intriguing setting to study cell elimination, given their vastly distinct compartments and hence likely differing elimination machineries. By definition, specialized cells bear distinct domains that differ in structure, function, subcellular architecture, and microenvironment. The compartmentalized nature of specialized cells is thus a major consideration in understanding how such cells are eliminated. Aside from neurons, other cell types exhibit morphological complexity and can die. Epithelial cells are also polarized into distinct structural and functional domains, and epithelial cell death is commonplace during development and tissue homeostasis, such as in the gut epithelium during inflammation.[7] The molecular mechanisms of compartment-specific regressive events, broadly, are still being elucidated.

Transport of cargo across the compartments of polarized cells such as neurons is important for the delivery of appropriate cargo to distant sites of function.[8] Such transport occurs via motors such as kinesins and dynein microtubule (MT) motors[9,10] that carry various cargo along the cytoskeleton. Cargo can include synaptic vesicles and organelles such as lysosomes and mitochondria.[11] How the regulation of transport of specific cellular cargo across different compartments drives specialized cell elimination is poorly understood.

Of known cell elimination programs, apoptosis is the best characterized, with defined morphological hallmarks and genetics, and the core components known to be conserved across species[1] and relevant for disease, such as in cancer therapeutics.[12] The genetic regulation of apoptosis was first delineated in the nematode *Caenorhabditis elegans*.[13,14] A cardinal molecular feature of apoptotic cell death is its regulation by cysteine proteases, caspases.[15,16] Caspases have both apoptotic and non-apoptotic functions.[15,17,18] Many caspase substrates have been implicated by *in vitro* proteomic studies,[19] though few caspase-regulated factors

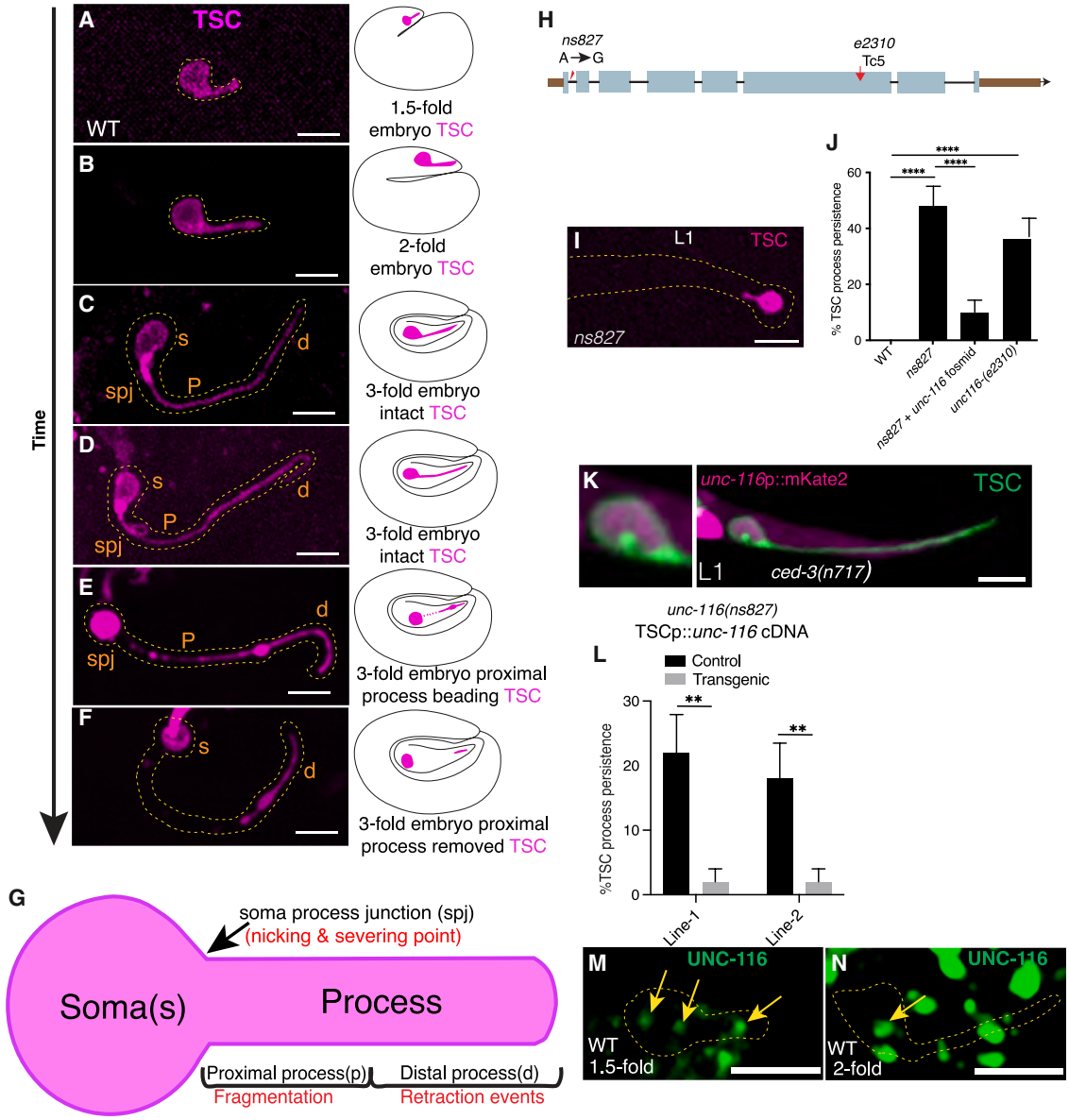

Figure 1. Spatiotemporal map of CCE and UNC-116/Kinesin-1 promotes CCE

(A–F) Steps of CCE, with schematic of embryo stages. The TSC is labeled with a membrane marker.

(A) 1.5-fold embryo stage (elongating TSC).

(B) 2-fold embryo stage (elongating TSC).

(C) An intact TSC, prior to CCE initiation.

(D) The TSC at the spj membrane nicking and severing stage.

(E) The TSC at the proximal process beading stage showing a rounded soma, a beading and fragmenting p, a distal node, and a retracting distal process tip.

(F) The TSC with the proximal process eliminated, with a remaining soma corpse and distal process remnant yet to be cleared. s, soma; p, proximal process; d, distal process; dN, distal node. *n* = 20 biologically independent animals with similar results.

(G) Spatiotemporal map of the TSC based on the stereotyped morphological changes observed during CCE. Red text indicates key CCE events in the relevant region. UNC-116/Kinesin-1 promotes CCE.

(H) *unc-116* gene structure.

(I) L1 *unc-116(ns827)* mutant.

(J) TSC elimination defects in indicated genotypes. *n*, sample sizes for statistics for each bar >50, with *n* referring to number of biologically independent animals.

(K) Expression of *unc-116* as seen using a transcriptional reporter for *unc-116* in TSC. *n* = 20 biologically independent animals with similar results.

(L) *unc-116(ns827)* mutant TSC-specific rescue. *n* sample sizes for statistics = 50 with *n* referring to number of biologically independent animals.

(legend continued on next page)

have been validated *in vivo*.[20,21] Several forms of non-apoptotic, caspase-independent cell death modalities have also been described,[22] and caspases have also been shown to play a localized role in developmental pruning.[3] In *C. elegans*, the main caspase is CED-3 (cell death abnormality),[23] which, in apoptotic cells, is regulated by a conserved pathway.[24]

We probed how fundamental features of polarized cells, such as the presence of disparate compartments, cargo transport, and local signaling events, cooperate to execute specialized cell elimination. We have previously introduced the embryonic cell death phenomenon, Compartmentalized Cell Elimination (CCE),[25] taking place in both the embryonic tail-spike epithelial cell (TSC) and sex-specific Cephalic male (CEM) sensory neurons of *C. elegans*. CCE is a caspase-dependent, non-canonically apoptotic, ordered and organized program whereby different cell compartments exhibit distinctive elimination morphologies that include those akin to developmental-region-specific neurite pruning.[3,26–28] The proximal process undergoes beading and fragmentation, and the d undergoes withdrawal or retraction.[28] We adopted an unbiased forward genetic approach in the nematode *C. elegans* to define fundamental principles of complex cell elimination and to identify novel regulators.

In this work, we describe how two kinesins compartment-specifically regulate CCE by transporting cytoprotective mitochondria. We show that UNC-116/Kinesin-1 is required for mitochondria to be transported out of the TSC process. The latter persists and harbors mitochondria in the absence of UNC-116. We also describe an atypical function of UNC-104/Kinesin-3, canonically known to carry synaptic vesicles, in mitochondrial transport, and its negative regulation by local function of CED-3/caspase. We show that local Ca^{2+} increase and CED-3 caspase activity are early CCE events. UNC-104/Kinesin-3 is negatively regulated, directly or indirectly, via proteolytic activity of CED-3/caspase. In the absence of CED-3/caspase, UNC-104/Kinesin-3 can transport mitochondria to take up Ca^{2+} via the mitochondrial Ca^{2+} uniporter (MCU)-1; although earlier steps are seen, CCE reverts to yield a surviving cell. In the presence of CED-3, local Ca^{2+} is seen, but UNC-104 is not seen, and CCE is completed. UNC-104 and UNC-116 have compartment-specific roles in the transport of mitochondria, with mitochondria promoting the preservation of the TSC in the relevant compartment. Our *in vivo* study reveals involvement of caspase activity and local Ca^{2+} signaling, differential region-specific contributions of mitochondria to cytoprotection, and atypical roles and regulation of kinesin motors, thereby broadening our understanding of how specialized cell elimination is orchestrated.

RESULTS

Higher-resolution analysis defines CCE degenerative dynamics in greater spatiotemporal detail

We performed a more detailed analysis of CCE of the TSC with higher spatial and temporal resolution. This has allowed us to define 5 TSC compartments with distinct degenerative morphologies across the sequential stages of CCE (Figure 1). As previously reported, the TSC has a cell body and a posteriorly directed MT-rich process that scaffolds the tail-tip[24,25,29] (Figures 1A–1C). Based on the subsequent degenerative dynamics of the TSC (Figures 1D–1F), we constructed a spatiotemporal map where distinct TSC cell regions are defined based on CCE steps (Figure 1G). From anterior to posterior, the key TSC regions are the soma (s), the soma-process junction (spj), the proximal process segment (p), and the distal process (d). The spj shows the first discernable sign of CCE, an initial membrane "nicking" event that is followed by "severing" of the process from the soma (membrane "nicking and severing," Figures 1D and 1G). This is followed by the "beading" stage (Figure 1E), where dramatic CCE events are evident in each TSC compartment.[25] The soma appears rounded and the proximal segment of the process (posterior to the membrane nicking-severing point) undergoes beading, membrane thinning, and fragmentation. The distal process develops a new compartment, the distal node, into which the rest of the distal process appears to retract. Ultimately, the proximal process is removed first (Figure 1F), and the soma and distal process remnant are cleared stochastically by different neighboring phagocytes.[24,25,29]

UNC-116/Kinesin-1 is required for proper CCE

We previously performed a forward genetic screen seeking to uncover factors regulating CCE, employing a membrane marker labeling the TSC (TSC-myrGFP).[25] From this screen, we recovered a mutant, *ns827*, in which the distal segment of the TSC process persists in first larval stage (L1) animals, when the TSC would normally be absent following its embryonic elimination (Figures 1H and 1I). Following whole-genome sequencing, single nucleotide polymorphism (SNP) mapping, and genomic DNA rescue, we identified the causative lesion to be an A to G splice donor after exon 1 of the gene *unc-116* (Figures 1H and 1J). The gene *unc-116* encodes the nematode homolog of the mammalian MT plus-end-directed motor KIF5/Kinesin-1.[30] We found *unc-116* to be expressed in the TSC by examining a transcriptional reporter for *unc-116* (*unc-116*pro::mKate2) (Figure 1K). We next performed cell-specific rescue experiments and found that UNC-116/Kinesin-1 functions in the TSC cell-autonomously (Figure 1L). We endogenously tagged UNC-116 with GFP via CRISPR-Cas9 and found that UNC-116 can be seen in the TSC s and process at the 1.5-fold embryo stage (Figures 1A and 1M; Video S1), but only in the s in the 2-fold embryo stage (Figures 1B and 1N; Video S1). This suggests that UNC-116/Kinesin-1 functions in transporting cargo from the TSC process toward the s.

UNC-116/Kinesin-1 transports mitochondria from the TSC process to the s to promote CCE

We next sought to identify the cargo UNC-116/Kinesin-1 and its role in CCE. Kinesin-1 is known to carry mitochondria,[31] and

(M and N) Endogenously tagged (GFP, green) UNC-116/Kinesin-1 showing localization in TSC distal process (magenta) at the 1.5-fold embryo stage (yellow arrow) (M) and 2-fold embryo stage (yellow arrow) (N). $n = 10$ biologically independent animals with similar results. Data in J and L are mean ± S.E.M. Statistics: two-tailed unpaied *t*-test. ns (not significant) $p > 0.05$, $^{*}p \leq 0.05$, $^{**}p \leq 0.01$, $^{***}p \leq 0.001$, $^{****}p \leq 0.0001$. Scale bar, 5m.
See also Video S1.

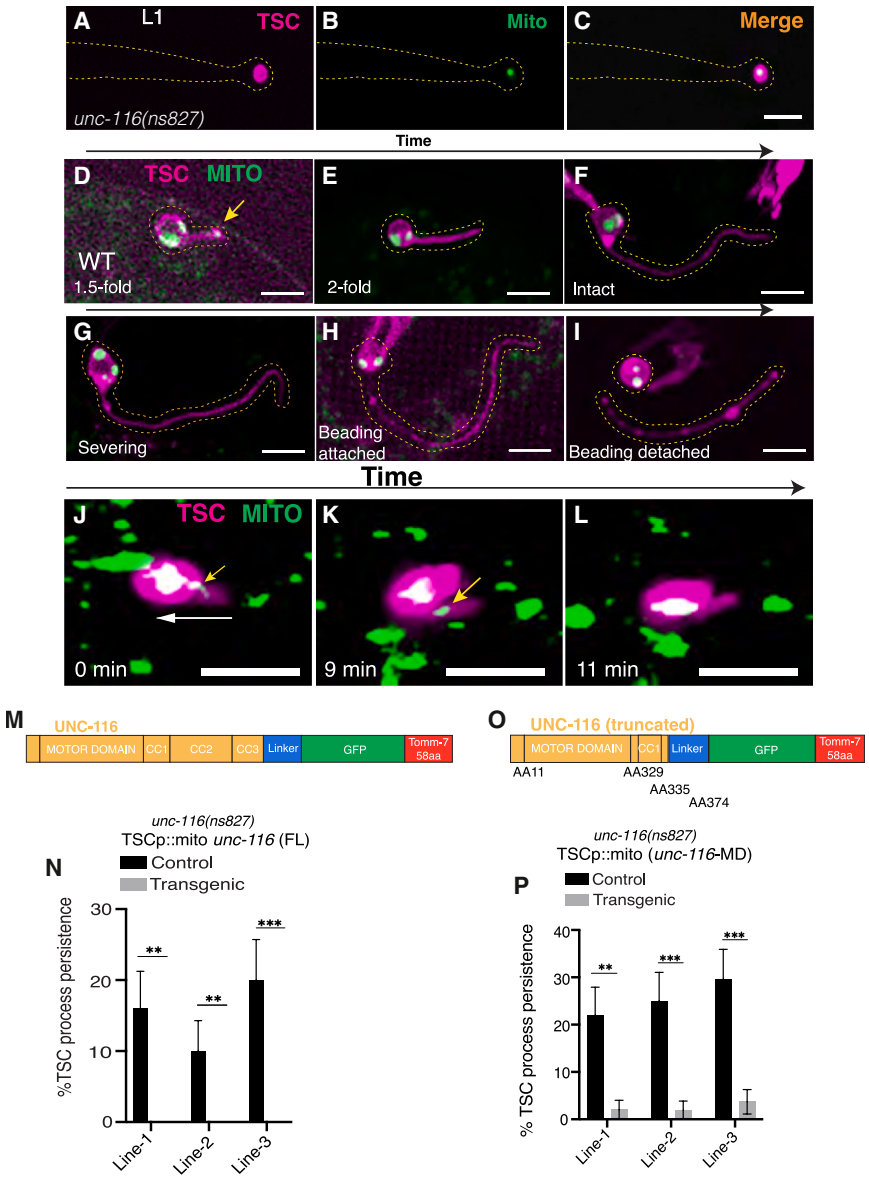

Figure 2. UNC-116/Kinesin-1 transports mitochondria from TSC process to s to promote CCE

(A–C) Image showing persisting mitochondria in L1 *unc-116(ns827)* (yellow arrow). *n* = 20 biologically independent animals with similar results.

(D–I) Mitochondria position across CCE stages in TSC in still images. *n* = 10 biologically independent animals with similar results.

(J–L) Frames (1, 4, and 8) from time-lapse video of mitochondrial transport in TSC (yellow arrow). *n* = 2 biologically independent animals with similar results.

(M–P) Mitochondria-specific rescues of *unc-116* mutant CCE defect using UNC-116-TOMM-7 chimeric proteins. Chimeric protein structure with full-length UNC-116 (M) and corresponding rescue graph (N); chimeric protein structure with tail-less UNC-116 (O) and corresponding rescue graph (P). *n*, sample sizes for statistics for each bar = 50 with *n* referring to number of biologically independent animals. Data in N and P are mean ± S.E.M. Statistics: two-tailed unpaired *t*-test. ns (not significant) $p > 0.05$, *$p \leq 0.05$, **$p \leq 0.01$, ***$p \leq 0.001$, ****$p \leq 0.0001$. Scale bar, 5μm.

See also Figures S1 and S2 and Videos S2 and S3.

mitochondria are associated with both cell survival and destruction.[32] Prior studies in *C. elegans* show UNC-116/Kinesin-1-dependent mitochondria to be important for neurite preservation following injury.[33] We asked whether mitochondria may be the relevant UNC-116/Kinesin-1 cargo in CCE. We generated a reporter for mitochondria (TSC-specific Mito-Matrix-GFP) against a red membrane marker and found mitochondria to be consistently present in the persisting TSC distal process remnant of *unc-116* mutants (30/30 animals) (Figures 2A–2C). We next tested the idea that this mutant defect is reflective of a mitochondrial transport defect that prevents mitochondria from their normal trajectory toward the s. We examined TSC-Mito::GFP in wild-type embryos first as still images at specific time points (Figures 2D–2I). We found mitochondria only in the process distally at or before the 1.5-fold embryo stage (Figures 1A and 2D) and not at later 2-fold (Figures 1B and 2E), or TSC intact (Figures 1C and 2F), nicking and severing (Figures 1D and 2G), and beading (Figures 1E, 2H, and 2I) CCE 3-fold embryo stages. We validated that mitochondria are indeed transported into the s in wild-type embryos via time-lapse imaging using light-sheet microscopy (Figures 2J–2L and S1; Videos S2 and S3). We next performed a rescue experiment using "TSCp::Mito-UNC-116" in which UNC-116/Kinesin-1 is linked to the outer membrane protein TOMM-7 such that this motor can only transport mitochondria as cargo, based on a previously used design[33] (Figures 2M and 2N). We saw strong rescue with "TSCp::Mito-UNC-116," suggesting that the transport of mitochondria by UNC-116/Kinesin-1 can specifically allow for proper CCE. We confirmed that this rescue is exclusively owed to the presence of mitochondria by testing a chimeric motor composed only of the motor domain and the first coiled-coil domain of UNC-116 (tail-less UNC-116) fused to TOMM-7 (Figures 2O and 2P). Here, too, we found significant rescue. This data, together with our observation that UNC-116 localizes at the tip of the TSC d at the 1.5-fold embryo stage (Figures 1A and 1M; Video S1), and then at the s later on at the 2-fold embryo stage (Figures 1B and 1N; Video S1), suggest that UNC-116 transports mitochondria from the TSC process to the s to promote CCE.

The TSC spj displays local CED-3 caspase activity and absence of mitochondria

Next, we examined our mitochondrial reporter at later embryonic stages. We found that as the TSC matures and

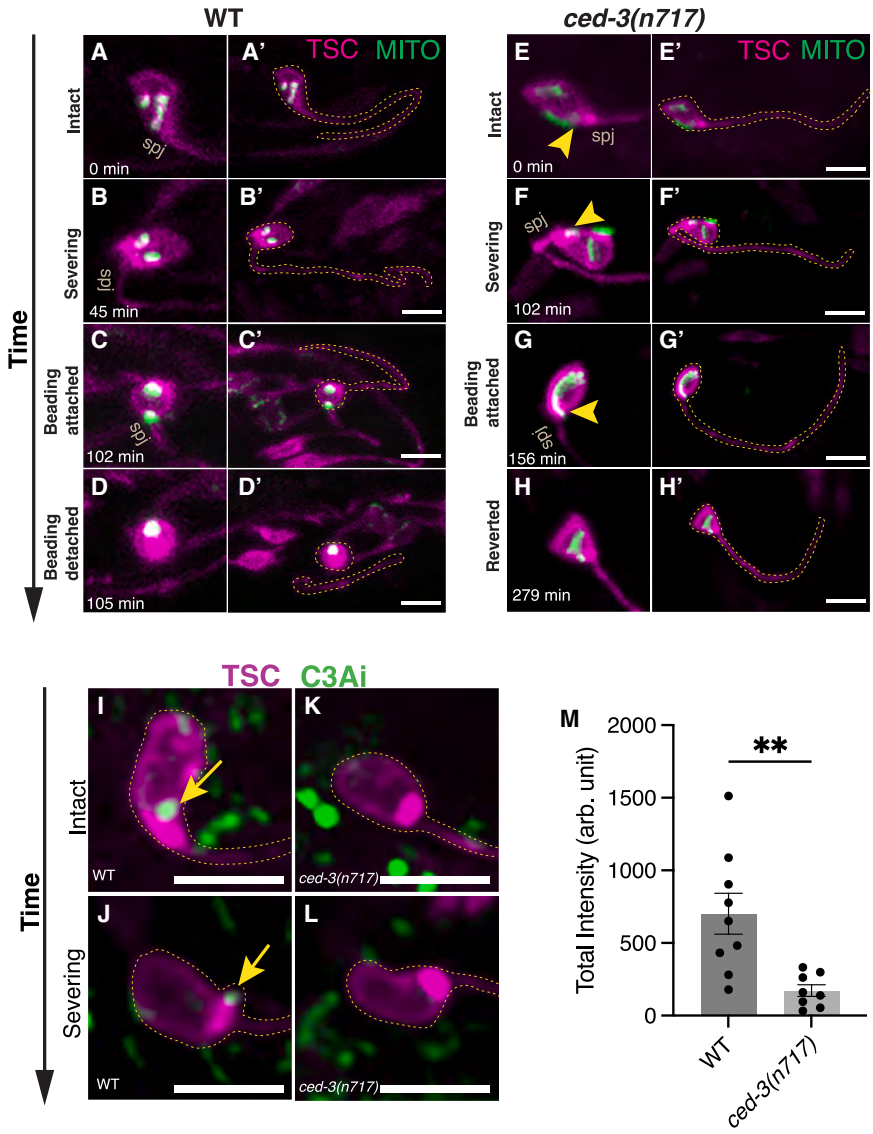

Figure 3. CED-3 caspase activity and absence of mitochondria at the TSC spj

(A–H′) Stills from video showing mitochondrial movement during CCE in wild-type (A–D′) and *ced-3(n717)* (E–H′) embryos, showing mitochondria entering spj in *ced-3(n717)* mutants (E–G′) (yellow arrowhead). $n = 2$ biologically independent animals with similar results.

(I–M) Caspase activity reporter GFP::C3Ai dynamics across CCE stages in wild type (I and J) (yellow arrow) and *ced-3(n717)* (K and L), and quantification of fluorescence intensity (M). $n = 20$ biologically independent animals with similar results. Data are mean ± S.E.M. Statistics: two-tailed unpaired *t*-test. ns (not significant) $p > 0.05$, $^{*}p \leq 0.05$, $^{**}p \leq 0.01$, $^{***}p \leq 0.001$, $^{****}p \leq 0.0001$. Scale bar, 5μm.

See also Videos S4 and S5.

CCE progresses, we do not observe mitochondria at the spj (Figures 1A–1F; 3A–3D′; Video S4). Importantly, the spj is the site of membrane "nicking and severing," whereby the TSC process is detached from the s. We hypothesized that mitochondria could preserve the spj if they are not transported away from this region. To test this idea, we examined a mutant for the main *C. elegans* caspase CED-3. CED-3 is essential for CCE, though it is regulated in a non-canonical manner, independent of EGL-1/BH3-only of the canonical apoptotic pathway.[34] In the absence of CED-3, TSC is intact in larva.[25,34] We examined TSC-Mito-GFP in null mutants for *ced-3* embryos (Figures 3E–3H′; Video S4) and made two striking observations. First, unlike the wild type (Figures 3A–3D′; Video S4), we find mitochondria at the spj. Second, we found the appearance of most CCE hallmarks—s rounding, proximal process beading, and distal node formation. However, the membrane nicking-severing event seen at the spj in wild-type embryos remains incomplete (Figures 1D, 3F, and 3F′), with only evidence of nicking, not progressing to detachment of the process from the s. Strikingly, the TSC appears to revert to its original intact morphology (Figures 3H and 3H′) and remains as such after hatching. To test directly whether region-specific caspase proteolytic activity of CED-3 is important for TSC spj membrane nicking-severing, we tested a TSC-specific GFP::C3Ai caspase activity reporter[35] in wild-type and *ced-3(n717)* mutants. We observed a sharp and specific signal at the spj in wild-type (Figures 3I, 3J, and 3M; Video S5) but not in *ced-3(n717)* (Figures 3K, 3L, and 3M; Video S5), suggesting that CED-3 caspase activity is at play at the spj during CCE. This suggests (1) removal of mitochondria from the spj is important for membrane nicking to severing, (2) that the membrane nicking-severing event is required for CCE to proceed to completion, and (3) that CED-3/caspase activity is important for this step.

UNC-104/Kinesin-3 promotes TSC survival and is negatively regulated by CED-3/caspase

We next tested the idea that CED-3/caspase regulates mitochondrial motor function to remove mitochondria from the spj and permit membrane nicking-severing. We have previously reported that the *ced-3(n2427)* hypomorph has a 40% CCE defect of inappropriate TSC persistence.[25] We tested for changes in TSC persistence with additional mutations in genes encoding different motor proteins.[36] We reasoned that, if a double mutant suppresses this *ced-3* hypomorphic CCE defect, the motor protein being tested is negatively regulated by CED-3/caspase. First we compared *ced-3(n2427)* hypomorph TSC persistence with that of single mutants for various mitochondrial motor-encoding genes[36] and only found TSC persistence in the *unc-116(ns827)* mutant as described above (Figure 4A). In addition to

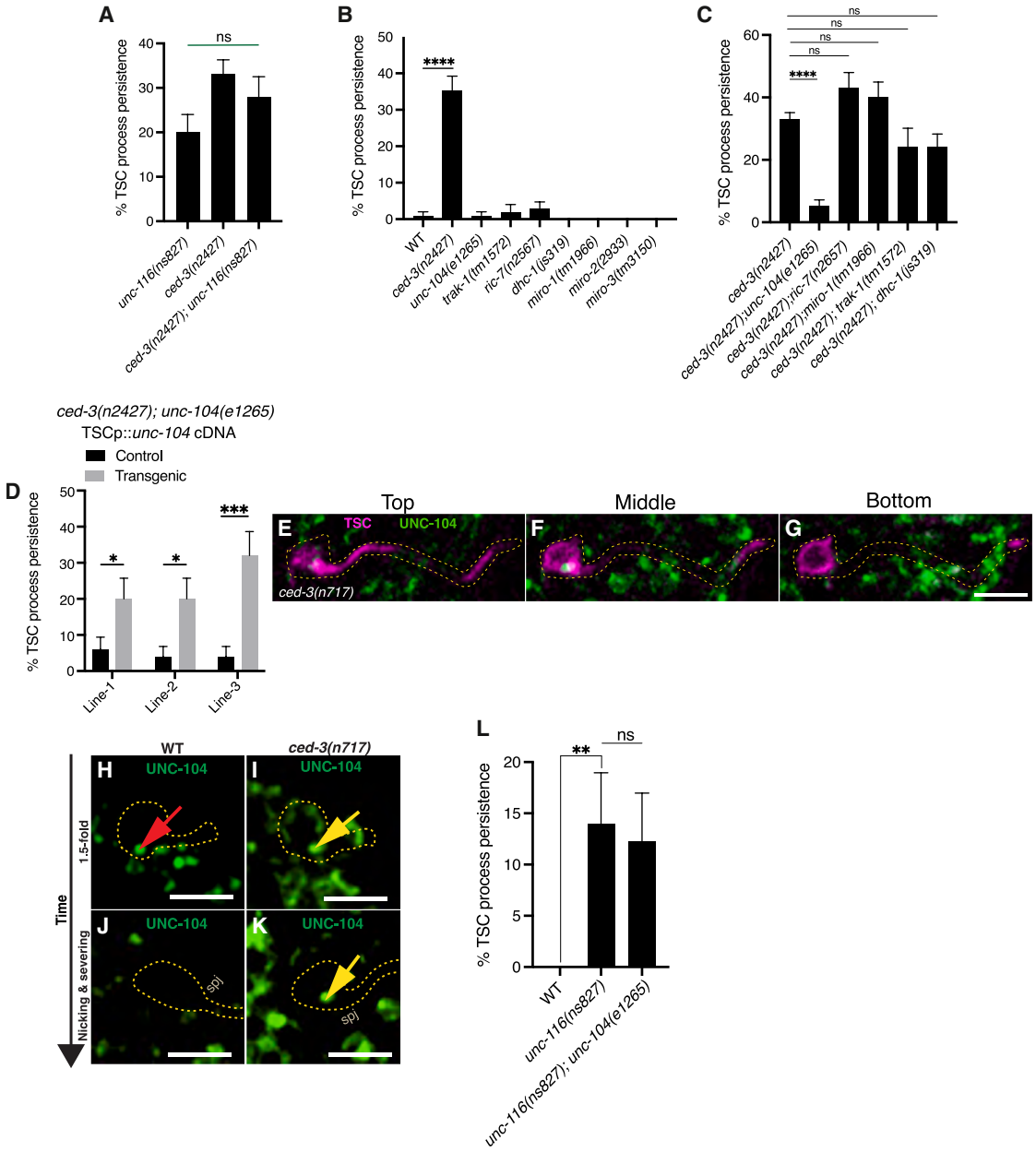

Figure 4. UNC-104/Kinesin-3 promotes TSC survival and is negatively regulated by CED-3/caspase

(A) Graph of TSC persistence of *unc-116(ns827), ced-3(n2427)*, and their double mutant.

(B) Graph of TSC persistence of single mutants for mitochondrial motor genes. *n*, sample sizes for statistics for each bar > 50 with *n* referring to number of biologically independent animals.

(C) Graph comparing TSC persistence *ced-3(n2427)* hypomorph with double mutants for motor genes. *n*, sample sizes for statistics for each bar > 50 with *n* referring to number of biologically independent animals.

(D) TSC-specific rescue of *unc-104*. *n*, sample sizes for statistics for each bar = 50 with *n* referring to number of biologically independent animals.

(E–G) Expression of UNC-104 in the TSC as shown by GFP insertion into endogenous locus of *unc-104*, green, UNC-104 TSC, magenta (E) top plane, (F) middle plane, and (G) bottom plane.

(H) S UNC-104 (endogenously tagged with GFP) signal in wild type at 1.5-fold embryo stage (red arrow).

(I) S/spj UNC-104 at 1.5-fold stage of *ced-3(n717)* (yellow arrow).

(J) S/spj UNC-104 at nicking-severing stage of *ced-3(n717)* (yellow arrow).

(K) Absence of UNC-104 signal in wild type at CCE nicking and severing stage. *n* = 10 biologically independent animals with similar results.

(L) Graph of TSC persistence in the *unc-116* single and *unc-116;unc-104* double mutants. *n*, sample sizes for statistics for each bar = 50 with *n* referring to number of biologically independent animals. Data in A–D and L are mean ± S.E.M. Statistics: two-tailed unpaired *t*-test. ns (not significant) $p > 0.05$, *$p \leq 0.05$, **$p \leq 0.01$, ***$p \leq 0.001$, ****$p \leq 0.0001$. Scale bar, 5m.

See also Video S6.

UNC-116, RIC-7 is essential for axonal mitochondrial localization.[33,36] However, we found no CCE defects in *ric-7(n2567)* mutants (Figure 4B) nor do we see a difference between *ced-3 (n2427)* and *ced-3(n2427);ric-7(n2567)* (Figure 4C). Next, we tested mutants for *miro-1*/Miro, *trak-1*/Trak, and *dhc-1*/dynein, other motors, and saw no CCE defect (Figure 4B). We then compared *ced-3(n2427)* hypomorph TSC persistence with double mutants for these various motors (Figure 4C).

Next, we widened our candidates to other MT motors. We considered UNC-104, the nematode homolog of mammalian Kinesin-3, known for its role in synaptic vesicle transport.[37] We did not see CCE defects in *unc-104(e1265)* single mutants (Figure 4B). However, double mutants for *ced-3(n2427); unc-104(e1265)* showed a significantly reduced CCE defect compared with the single mutant *ced-3(n2427)* (Figure 4C). We re-introduced TSC-specific *unc-104* into the double mutant and found TSC persistence back to the level of the *ced-3(n2427)* single mutants, suggesting a cell-autonomous function of UNC-104 to promote CCE in the absence of CED-3 (Figure 4D). Next, we sought to view *unc-104* expression and how CED-3 may affect the UNC-104 protein. To this end, we generated endogenously tagged (GFP at C terminus) *unc-104* using CRISPR-Cas9 in *ced-3(n717)* mutants. We found that UNC-104 is indeed expressed in the TSC (Figures 4E–4G). As expected, the UNC-104::GFP signal persisted in the TSC spj across stages in *ced-3(n717)* mutants (Figures 4I–4K; Video S6), which is consistent with a lack of caspase activity in *ced-3(n717)* mutants at this region (Figures 3K and 3L). As a control, we looked at UNC-104::GFP in the wild-type background in which CED-3 would be present, where we see local caspase activity in the spj consistently (Figures 3I and 3J). As expected, we did not see the UNC-104 signal at the spj at CCE onset (Figure 4J; Video S6). Surprisingly, at earlier stages, we do see the UNC-104 signal in the TSC. However, this is remote from the spj at other sites in the s (Figure 4H; Video S6). These data suggest that CED-3 promotes CCE by negatively regulating UNC-104/Kinesin-3 protein at the TSC spj, and that this may be spatially and temporally regulated.

UNC-104/Kinesin-3 transports mitochondria in the absence of CED-3/caspase

Next, we tested whether mitochondria are a bona fide cargo of UNC-104/Kinesin-3 in the TSC, given that UNC-104 is a more established motor for synaptic vesicles.[37] We adopted three strategies. First, we generated "TSCp::Mito-UNC-104" where, as above for UNC-116, UNC-104 is linked to the outer membrane protein TOMM-7 to transport only mitochondria. We introduced TSCp::Mito-UNC-104 into *ced-3(n2427);unc-104(e1265)* mutants and found significant rescue (Figure 5A). Second, we then tested for colocalization between mCherry-tagged UNC-104/Kinesin-3 and MitoGFP in *ced-3* mutant L1 larva (Figures 5B–5D) and found colocalization specifically at the spj. Interestingly, time-lapse imaging shows that in the TSC s, UNC-104 approaches mitochondria that are separating, associating with each fragment consecutively, appearing to further their separation (Figures 5E–5I; Video S7). Third, we looked at TSC-MitoGFP in *ced-3(n717)* larva, in which UNC-104/Kinesin-3 is presumed to be stable, and found mitochondria in the process (Figures 5J and 5N). We looked at a *ced-3(n717);unc-116 (ns827)* double mutant, where mitochondria also cannot exit the process into the s. Mitochondria were heavily enriched in the process in this background (Figures 5K and 5N). We next compared this to a triple mutant for *ced-3(n717);unc-104 (e1265);unc-116(ns827)* (Figures 5L and 5N) and found mitochondria to be in significantly lower number, suggesting that UNC-104/Kinesin-3 is necessary for the enhanced mitochondrial presence in the double mutant. We also looked at *ced-3(n717); dhc-1(js319);unc-116(ns827)* but did not find a decrease in mitochondria number in the process (Figures 5M and 5N). Our interpretation of the data in Figures 5K–5M is schematically represented in Figure S2. We suggest that UNC-104 can transport mitochondria to the TSC spj in the absence of CED-3 in the embryo (Figures S2A and S2B) and can transport mitochondria farther into the process as the TSC matures to L1 (Figure S2C). This transport is balanced by s-ward transport of mitochondria by UNC-116. In the absence of UNC-116, mitochondria can enter the process via UNC-104 but cannot exit, leading to accumulation of mitochondria in the process (Figure S2D). In the absence of UNC-104, no new mitochondria enter, and mitochondria already present remain in the absence of UNC-116 (Figure S2E). Loss of DHC-1 does not affect the number of mitochondria in the TSC process (Figure S2F). Collectively, these data support a model in which UNC-104/Kinesin-3 can carry mitochondria in the TSC in the absence of CED-3/caspase.

Mitochondria are protective via Ca^{2+} uptake in a compartment-specific manner

Our data suggest that mitochondria are protective against CCE through roles in the TSC process and TSC spj. We also propose that transport by UNC-116/Kinesin-1 and UNC-104/Kinesin-3 is important to regulate cell elimination via mitochondrial transport. We next addressed what aspect of mitochondrial function contributes to this protective role. We first tested whether mitochondrial energy production gives mitochondria the ability to preserve the TSC. We tested *clk-1*, which encodes co-enzyme Q, a component of the oxidative phosphorylation pathway,[38] against the *ced-3(n2427)* hypomorphic background (Figure 6A). Surprisingly, the double mutant had the same proportion of CCE-defective animals as the *ced-3* hypomorph, suggesting mitochondrial energy production may not explain why mitochondria need to be removed from the process for its elimination. We next tested an alternative hypothesis that the ability of mitochondria to act as Ca^{2+} sinks may give them cell-protective capability. We therefore tested a mutant for the gene encoding MCU-1 (mitochondrial calcium uniporter), a Ca^{2+}-selective mitochondrial ion channel[39] in the *ced-3* hypomorphic background. Interestingly, in this instance, we did see a partial, but significant, suppression of the *ced-3* hypomorphic CCE defect (Figure 6B). This suggests that the ability of mitochondria to import cytosolic Ca^{2+} may give it a protective role in CCE. Supporting this, when we re-introduced TSC-specific *mcu-1* in a *ced-3(n2427);mcu-1 (ju1154)* double mutant, we found the phenotype to be rescued (Figure 6C).

Our genetics suggest a role for Ca^{2+} in CCE, suggesting changes in Ca^{2+} levels are regulated by mitochondrial Ca^{2+} uptake. We examined a TSC-specific cytosolic GCaMP5a[40] (genetically encoded calcium indicator) reporter to visualize Ca^{2+} spikes in the TSC. Interestingly, in wild-type embryos, we detected local cytosolic Ca^{2+} spikes at the spj most visible in the

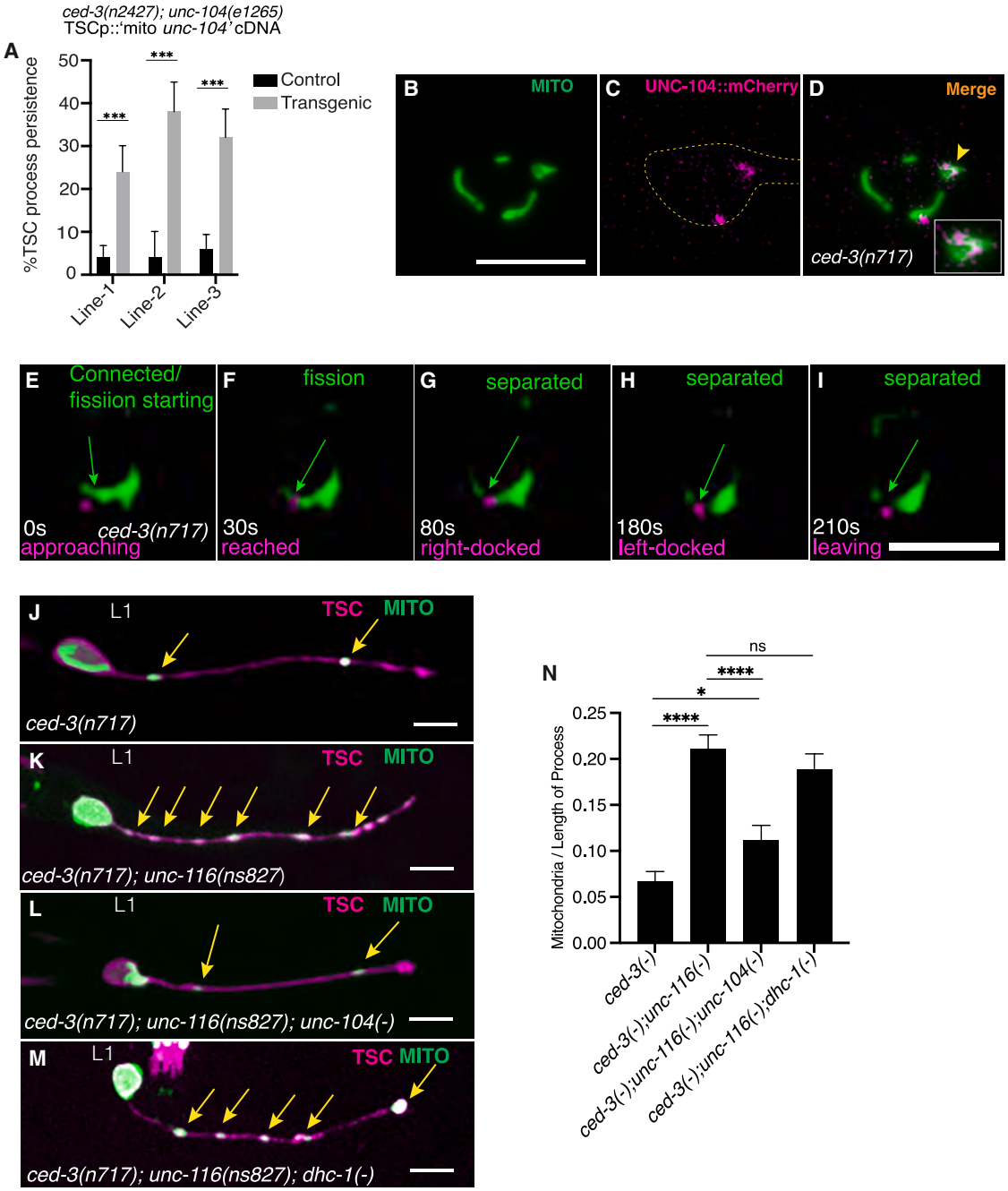

Figure 5. UNC-104/Kinesin-3 transports mitochondria in the absence of CED-3/caspase

(A) TSC mitochondria-specific rescue of *unc-104* mutant CCE defect. *n*, sample sizes for statistics for each bar = 50 with *n* referring to number of biologically independent animals.

(B–D) Colocalization of UNC-104 and mitochondria in L1 larva of *ced-3(n717)*. *n* = 15 biologically independent animals with similar results.

(E–I) Time-lapse of co-labeled UNC-104 (magenta) and mitochondria (green) as seen in the TSC s, showing transient association of UNC-104 with apparently fragmenting mitochondria (green arrow), *n* = 3.

(J) Presence of mitochondria in the TSC process in *ced-3(n717)* single mutants (yellow arrow).

(K) Enrichment of mitochondria in TSC process of *ced-3(n717);unc-116(ns827)* double mutants (yellow arrow).

(L) Loss of this enrichment of mitochondria in TSC process of *ced-3(n717);unc-116(ns827);unc-104(e1265)* triple mutants (yellow arrow).

(M) Enrichment of mitochondria in TSC process of *ced-3(n717);unc-116(ns827);dhc-1(js319)* triple mutants (yellow arrow).

(N) Graph for (J)–(M). *n*, sample sizes for statistics for each bar = 30 with *n* referring to number of biologically independent animals. Data in A and N are mean ± S.E.M. Statistics: two-tailed unpaired *t*-test. ns (not significant) $p > 0.05$, *$p \leq 0.05$, **$p \leq 0.01$, ***$p \leq 0.001$, ****$p \leq 0.0001$. Scale bar, 5μm.

See also Figure S2 and Video S7.

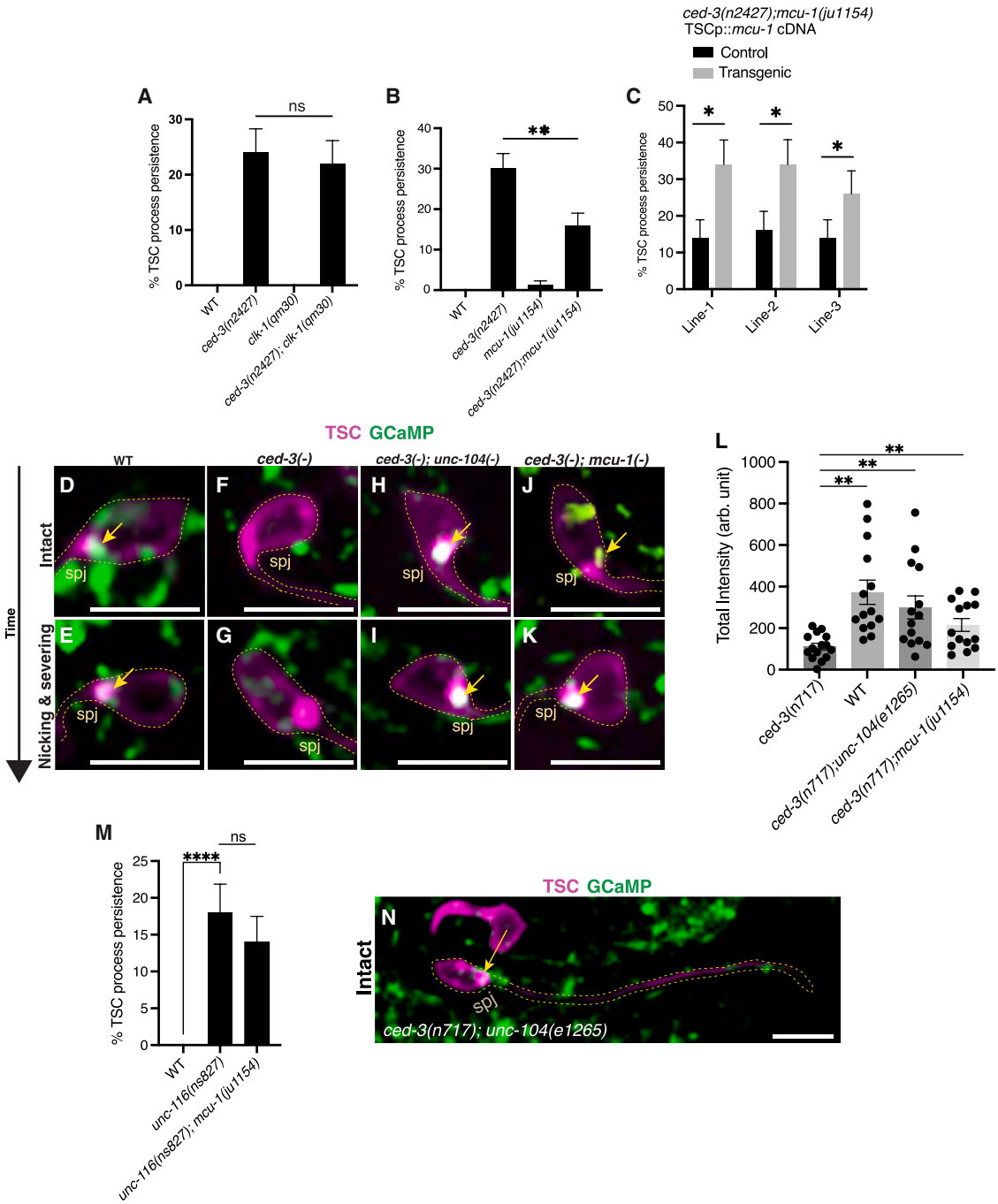

Figure 6. Compartment-specific protective function mitochondria via local Ca^{2+} uptake

(A) Graph showing CLK-1 does not regulate CCE. *n*, sample sizes for statistics for each bar >50 with *n* referring to number of biologically independent animals.

(B) Graph showing MCU-1/MCU prevents CCE. *n*, sample sizes for statistics for each bar >50 with *n* referring to number of biologically independent animals.

(C) Graph showing MCU-1 functions in the TSC cell-autonomously to repress CCE. *n*, sample sizes for statistics = 50 with *n* referring to number of biologically independent animals.

(D–K) Localization of GCaMP5 Ca^{2+} sensor in TSC at the intact and nicking/severing stage of CCE in wild type (yellow arrow) (D and E), *ced-3(n717)* (F and G), *ced-3(n717);unc-104(e1265)* double mutant (yellow arrow) (H and I), and *ced-3(n717);mcu-1(ju1154)* double mutant (yellow arrow) (J and K).

(L) Quantification of fluorescence intensity of (D)–(K). *n* = 14 biologically independent animals with similar results.

(M) Graph comparing TSC persistence between *unc-116(ns827)* single and *unc-116(ns827);mcu-1(ju1154)* double mutants, *n*, sample sizes for statistics > 50 with *n* referring to number of biologically independent animals.

(N) GCaMP reporter as in whole TSC to show lack of signal in process but presence in spj (yellow arrow). Data in A–C and L–M are mean ± S.E.M. Statistics: two-tailed unpaired *t*-test. ns (not significant) $p > 0.05$, $^{*}p \leq 0.05$, $^{**}p \leq 0.01$, $^{***}p \leq 0.001$, $^{****}p \leq 0.0001$. Scale bar, 5μm.

See also Figure S3 and Videos S8 and S9.

intact to membrane nicking-severing stage (Figure 6D, 6E, and 6L; Video S8). We did not see such a signal in *ced-3* mutants (Figures 6F, 6G, and 6L; Video S8). In both the *ced-3(n2427); unc-104(e1265)* double mutants (Figures 6H, 6I, and 6L; Video S8) and *ced-3(n2427);mcu-1(ju1154)* double mutants (Figures 6J, 6K, and 6L; Video S8), the local GCaMP signal was restored. These data suggest that local Ca^{2+} increase at the spj is involved in CCE and is prevented by mitochondrial Ca^{2+} uptake and that UNC-104 promotes mitochondrial transport to the spj in the absence of CED-3. In the presence of CED-3, mitochondria remain remote from the spj, permitting local Ca^{2+} increase, membrane nicking-severing, and the progression of CCE. We propose that the TSC spj is preserved in the absence of CED-3 by mitochondrial Ca^{2+} uptake facilitated by UNC-104.

We tested whether the TSC d persistence of *unc-116* mutants is suppressed by loss of *mcu-1* as with the *ced-3* hypomorph. Surprisingly, and contrary to our original model, we found no difference between *unc-116* single and *unc-116;mcu-1* double mutants (Figure 6M), suggesting that the protective nature of mitochondria in the d remnant of *unc-116* mutants is not a function of mitochondria Ca^{2+} uptake as for *ced-3* mutants. This is, however, consistent with our observation that we did not see GCaMP signal in the TSC d (Figure 6N; Video S9). We do further note that, as we have previously shown,[25] *ced-3* hypomorphs have a range of CCE defects, including an intact proximal process alone. Interestingly, this lone process harbors mitochondria (Figure S3) and, as shown, the overall phenotype is partially reduced with the additional loss of *mcu-1* (Figure 6B) but not *clk-1* (Figure 6A). In both these double mutants, UNC-116 is presumably functional such that it can transport mitochondria to the s. We note that the CCE defect of the *unc-116* mutants and *ced-3(n2427);unc-116(ns827)* double mutants are not significantly different (Figure 4A). This is consistent with the model that mitochondrial transport to the s via UNC-116 occurs prior to CED-3-dependent CCE onset.

The TSC process is preserved if UNC-116 is unable to transport mitochondria out of the process toward the s. The localizations of UNC-116 and UNC-104, two MT plus-end-directed proteins, are consistent with a model of compartment-specific cytoprotective capabilities of mitochondria. UNC-116 is present at the TSC d tip early on (Figures 1A and 1M), and then at the s later (Figures 1B and 1N), and UNC-104 (Figures 4I and 4K) at the spj in *ced-3* mutants. Given our observation that loss of *unc-104* suppresses the *ced-3* hypomorph CCE defect, we examined whether TSC process persistence of *unc-116* mutants is also suppressed by loss of *unc-104*. Interestingly, we found no difference in TSC persistence in the *unc-116* single and *unc-116; unc-104* double mutants (Figure 4L). This suggests that UNC-104's protective role in CCE requires an absence of CED-3 and that the absence of UNC-116 is not sufficient. It also supports the idea that the contributions of UNC-104 and UNC-116 to CCE regulation may be compartment specific.

Compartment specificity of MT polarity, mitochondrial function, and transport dynamics

To further understand the differential contributions of UNC-104 and UNC-116 in TSC elimination, we evaluated MT orientation in the TSC process compartments. We generated a TSC-specific reporter for the MT plus-end-binding protein EBP-2.[41] Interestingly, we observed compartment-specific differences in MT polarity. We found EBP-2 comets to be directed both to and away from the s, close to the spj. Further distally, we find EBP-2 comets directed toward the s. Interestingly, at the very distal tip of the TSC process where it forms the spike, we observe plus-end-out polarity (Figures 7A and 7B; Video S10). This region-specific diversity on MT polarity is likely related to the function and elimination modality of each compartment. Interestingly, mixed MT polarity, as seen proximally, is a characteristic of dendrite architecture, and CCE is also seen in CEM sensory neurons, which have single dendrites.[25]

Collectively, our data allow us to construct a model (Figure 7C) whereby the elimination of the TSC is achieved by compartment-specific regulatory events involving mitochondrial transport. Mitochondria are transported out of the process via UNC-116/Kinesin-1 and kept remote from the spj via direct or indirect inhibition of UNC-104/Kinesin-3 by CED-3/caspase. At the spj, mitochondria take up Ca^{2+}, preventing membrane nicking-severing and the progression of CCE. Here, two kinesins play compartment-specific roles, with UNC-104/Kinesin-3 in an atypical role as a mitochondrial motor. We propose that while UNC-116 can transport mitochondria toward the s along the full length of the process, how far UNC-104 can traffic mitochondria into the process depends on its developmental stage, mainly restricted to the spj in the embryo. Our work highlights region-specific contributions of differential MT orientation, mitochondrial transport and protective capacity, local caspase function, and Ca^{2+} in CCE.

DISCUSSION

Previous work in *C. elegans* demonstrates that, following injury, mitochondria can protect axons from degeneration[33] and can aid in regeneration.[42] Mitochondria can protect against cell death through elevated mitochondrial activity,[43] as well as via enhanced mitochondrial Ca^{2+} uptake.[44] Conversely, excess mitochondrial Ca^{2+} uptake, can also trigger cell death.[45] Here, we present a role for mitochondria in cytoprotection during development through local Ca^{2+} uptake (Figure 6). We also introduce the intriguing idea that mitochondria contribute differently to the preservation of the distinct cell compartments, highlighting further the compartment-specific regulation of specialized cell death. We note that mitochondria are protective for the TSC d and spj, but not the s. This may be due to fundamental differences between these cell compartments structurally and how they respond to mitochondrial function. We also observe that the protective impact of mitochondria depends on the cell compartment in which the mitochondria are located: distal mitochondria can only protect the cell locally and mitochondria in the spj can save the entire cell. One reason for these differences may be the distinctive MT orientation at the different segments of the TSC process. Compartment-specific specialization at the level of the cytoskeleton may dictate the importance of that domain to CCE and how its dismantling is regulated. We speculate that there is a correlation between cytoskeleton function and elimination strategy for different TSC compartments. The spj has mixed MT polarity; farther distal it is plus-end-in, and distal-most is plus-end-out. Each region is eliminated in a different way, at a different time.

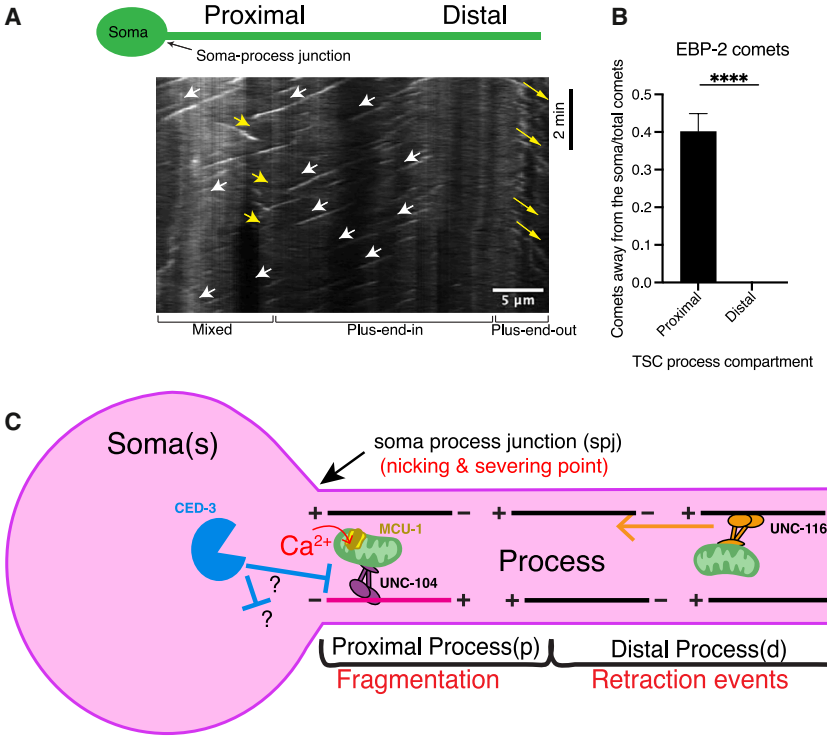

Figure 7. Compartment specificity of MT polarity in the TSC and model for mitochondrial function and transport dynamics during CCE

(A) Kymograph of TSC promoter-driven EBP-2::GFP in *ced-4(n1162)* mutant L1 larvae. White arrows mark EBP-2 comets directed toward the TSC s; yellow arrows mark EBP-2 comets directed away from the TSC s; thin yellow arrows, EBP-2 comets plus-end-out of distal-most tip. Scale bar, 5µm.

(B) Graph of ratio of comets directed away from the TSC s versus total number of comets. $n = 10$ biologically independent animals with similar results. Data are mean ± S.E.M. Statistics: two-tailed unpaired *t*-test. ns (not significant) $p > 0.05$, $^{*}p \leq 0.05$, $^{**}p \leq 0.01$, $^{***}p \leq 0.001$, $^{****}p \leq 0.0001$.

(C) Model for roles of UNC-116/Kinesin-1 and UNC-104/Kinesin-3 in transporting mitochondria in the context of CCE. UNC-116/Kinesin-1 transports mitochondria out of the TSC process toward the s to promote TSC process elimination during CCE. CED-3/caspase ensures mitochondria remain remote from the spj and in the s by negatively regulating UNC-104/Kinesin-3. This permits localized Ca^{2+} spiking at the spj and spj membrane severing during CCE. In the absence of CED-3/caspase, UNC-104/Kinesin-3 performs a non-canonical function of short-range mitochondrial transport to the spj. Mitochondria so-transported take up cytosolic Ca^{2+} via the uniporter MCU-1 and CCE can reverse resulting in survival of the TSC. See also Video S10.

Our work also highlights the importance of local Ca^{2+} and region-specific caspase activity in promoting CCE (Figure 4I). The precise role of this Ca^{2+} in CCE is yet to be determined and is an important future direction. Whether CED-3/caspase targets UNC-104/Kinesin-3 for cleavage directly or via a partner or adaptor remains to be examined. Our observation of region-specific caspase activity is consistent with our prior studies showing a range of compartment-specific defects of the *ced-3* hypomorph, suggesting that CED-3/caspase acts independently in the different TSC sub-compartments.[25] Region-specific pruning has also been reported to be regulated by caspase gradients.[4] Uncovering what potentiates region-specific caspase activity and the relevant caspase substrates merits future study. The reversible nature of the caspase-independent steps of the non-canonically apoptotic program of CCE presents us with a new setting in which to understand the molecular mechanism of cellular resilience. Interestingly, neuronal apoptosis has been shown to be reversible.[46]

We present in this study atypical roles for two well-known MT motors. Kinesin-1 is classically known as an anterograde motor.[31] In *C. elegans*, UNC-116/Kinesin-1[33] maintains mitochondrial density in motor neurons and touch receptor neurons[33,47] via anterograde axonal transport, and protects the axon from degeneration following injury.[33] Our work in the TSC presents UNC-116 in an essentially opposite role, serving in region-specific exclusion of cytoprotective mitochondria by transporting mitochondria s-ward (Figure 7C).

We also present UNC-104/Kinesin-3 in an atypical role of carrying mitochondria as cargo (Figure 7C). UNC-104 is the founding member of the kinesin-3 family[37] canonically known to transport much smaller pre-synaptic vesicles.[48] Mammalian Kinesin-3/KIF1A is neuron specific and functions in the fast anterograde axonal transport of synaptic vesicle precursors.[48] There is a precedent for other members of the kinesin-3 family to carry cargo other than synaptic vesicles, including dense core granules by neuron-specific KIF1A,[49] Nkin2/Nkin3 in *Neurospora crassa*,[50] and KLP-6[51] in *C. elegans*. KIF1B has been previously shown to localize to mitochondria *in vivo*.[52] Prior studies in *C. elegans* have shown that mitochondrial localization is not altered in neurons of the *unc-104* mutant.[33] Moreover, the cargo-binding tail domains of Kinesin-3 family members such as KLP-6 and KIF1Balpha are distinct from KIF1A.[53] As such, previous studies do not support the notion that UNC-104 can transport mitochondria in neurons tested thus far. How *C. elegans* UNC-104/Kinesin-3 associates with mitochondria remains an open question for future studies. It is possible that this specific cargo transport role of UNC-104 is exclusive to the TSC in *ced-3* mutants. Further studies in various neuron subtypes, including the CEM neurons, will be interesting to pursue to further investigate the versatility of UNC-104 as a motor. It is possible that it acts in conjunction with an adaptor specific to the TSC. Structure-function studies of UNC-104/Kinesin-3's conserved pleckstrin homology (PH) domain,[54] which acts as a lipid-binding domain for cargo, may provide insights into potential cargo adaptability of this kinesin family. Selective KIF1A cargo trafficking has been suggested to be regulated by specific adaptors, such as motor-cargo linkage proteins or even other motors, post-translational modification of the motor,[53,55,56] or dimerization/clustering.[57] Interestingly, data suggest that UNC-104 in *C. elegans* mechanosensory neurons is degraded when

not bound to cargo.[58] We also observe a potentially new role of UNC-104, wherein UNC-104, via its short-range transport function, follows and cooperates with the mitochondrial fission machinery[59] to ensure mitochondrial fragments generated do not re-connect.

Given that UNC-104 and UNC-116 are both MT plus-end-directed motors, an outstanding question is why and how these motors occur at specific poles of the TSC moving toward opposing cell compartments (Figures 1M, 4I, and 7). The differential MT orientation in different TSC process segments offers an explanation as to how this is possible. Identifying what cues specifically direct transport toward a particular cell region is an important future goal. In addition, the lack of involvement of DHC-1/dynein was surprising but may explain why we observe UNC-116 and UNC-104 in atypical roles in the context of the TSC.

We note that the TSC, while polarized, is an epithelial cell and not a neuron. The TSC epithelial cell is indeed functionally and physiologically distinct from neurons, serving a physical scaffolding role for the worm tail rather than in transmitting information by generating action potentials or forming synapses. Neurons are also subject to death or regression, both developmentally[2] and under pathological[60] or injury contexts.[61] Like neurons, the TSC is morphologically complex and is a valuable platform for studying facets of neurons pertaining to their structural complexity, such as organellar transport[62,63] and compartmentalization.[8,64] Additionally, we have previously shown that the *C. elegans* hermaphrodites' CEM sensory neurons also undergo CCE.[25] Of note, the hermaphrodite CEM neurons die before their axon can form, with only a single dendrite that shows CCE hallmarks of the TSC process. Future work exploring the roles of mitochondrial transport in the axon and dendrite during CEM neuron death will further illuminate our understanding of specialized cell death in the specific context of neurons.

RESOURCE AVAILABILITY

Lead contact

Further information and requests for resources should be directed to, and will be fulfilled by, the lead contact, Piya Ghose (piya.ghose@uta.edu).

Materials availability

All *C. elegans* stocks and reagents used in this study will be made available upon request without any restriction.

Data and code availability

- All data reported in this paper will be shared by the lead contact upon request.
- This paper does not report original code.
- Any additional information required to reanalyze the data reported in this paper is available from the lead contact upon request.

ACKNOWLEDGMENTS

Some strains were provided by the CGC, which is funded by NIH Office of Research Infrastructure Programs (P40 OD010440). P. Ghose is funded by a National Institutes of Health – National Institute of General Medical Sciences Maximizing Investigators' Research Award (MIRA) (R35GM142489) and is a Cancer Prevention and Research Institute of Texas (CPRIT) Scholar in Cancer Research (RR100091). This work was also supported by NIH MIRA grants R35GM151199 to P.K.S., R35GM128885 to M.W.P., and a CPRIT Scholar in Cancer Research (RR160053) and NIH grants R01HD103610 and R35NS105094 to S.S. We thank Nathan Rather for technical assistance. We thank the Ghose Lab for comments on the manuscript.

AUTHOR CONTRIBUTIONS

R.S. and P. Ghose designed the experiments and wrote the paper. R.S., A.E., S.P., P.K.S., and P. Gaddipati performed experiments and analyzed data. A.E. assisted in editing the paper. G.C. provided significant technical assistance. R.S. and P. Ghose conceptualized the study, with early contributions from M.W.P. and S.S. and early resources from S.S.

DECLARATION OF INTERESTS

The authors declare no competing interests.

STAR★METHODS

Detailed methods are provided in the online version of this paper and include the following:

- KEY RESOURCES TABLE
- EXPERIMENTAL MODEL AND STUDY PARTICIPANT DETAILS
  - *C. elegans* culture
- METHOD DETAILS
  - Germline transformation and rescue experiments
  - Primers and plasmid construction
  - CRISPR-Cas9 genome editing
  - Scoring of TSC/CCE defects
  - Mutagenesis and mutant identification
  - Microscopy and image processing
- QUANTIFICATION AND STATISTICAL ANALYSES
  - Quantification of mitochondria
  - Quantification of Fluorescence Intensity
  - Statistics and reproducibility

SUPPLEMENTAL INFORMATION

Supplemental information can be found online at https://doi.org/10.1016/j.cub.2025.08.065.

Received: October 11, 2024
Revised: June 2, 2025
Accepted: August 28, 2025
Published: September 19, 2025

REFERENCES

1. Fuchs, Y., and Steller, H. (2011). Programmed cell death in animal development and disease. Cell *147*, 742–758. https://doi.org/10.1016/j.cell.2011.10.033.
2. Yamaguchi, Y., and Miura, M. (2015). Programmed cell death in neurodevelopment. Dev. Cell *32*, 478–490. https://doi.org/10.1016/j.devcel.2015.01.019.
3. Schuldiner, O., and Yaron, A. (2015). Mechanisms of developmental neurite pruning. Cell. Mol. Life Sci. *72*, 101–119. https://doi.org/10.1007/s00018-014-1729-6.
4. Maor-Nof, M., and Yaron, A. (2013). Neurite pruning and neuronal cell death: spatial regulation of shared destruction programs. Curr. Opin. Neurobiol. *23*, 990–996. https://doi.org/10.1016/j.conb.2013.06.007.
5. Faust, T.E., Gunner, G., and Schafer, D.P. (2021). Mechanisms governing activity-dependent synaptic pruning in the developing mammalian CNS. Nat. Rev. Neurosci. *22*, 657–673. https://doi.org/10.1038/s41583-021-00507-y.

6. Neniskyte, U., and Gross, C.T. (2017). Errant gardeners: glial-cell-dependent synaptic pruning and neurodevelopmental disorders. Nat. Rev. Neurosci. *18*, 658–670. https://doi.org/10.1038/nrn.2017.110.
7. Buckley, C.E., and St Johnston, D. (2022). Apical-basal polarity and the control of epithelial form and function. Nat. Rev. Mol. Cell Biol. *23*, 559–577. https://doi.org/10.1038/s41580-022-00465-y.
8. Terenzio, M., Schiavo, G., and Fainzilber, M. (2017). Compartmentalized Signaling in Neurons: From Cell Biology to Neuroscience. Neuron *96*, 667–679. https://doi.org/10.1016/j.neuron.2017.10.015.
9. Reck-Peterson, S.L., Redwine, W.B., Vale, R.D., and Carter, A.P. (2018). The cytoplasmic dynein transport machinery and its many cargoes. Nat. Rev. Mol. Cell Biol. *19*, 382–398. https://doi.org/10.1038/s41580-018-0004-3.
10. Verhey, K.J., Kaul, N., and Soppina, V. (2011). Kinesin assembly and movement in cells. Annu. Rev. Biophys. *40*, 267–288. https://doi.org/10.1146/annurev-biophys-042910-155310.
11. Caviston, J.P., and Holzbaur, E.L.F. (2006). Microtubule motors at the intersection of trafficking and transport. Trends Cell Biol. *16*, 530–537. https://doi.org/10.1016/j.tcb.2006.08.002.
12. Johnstone, R.W., Ruefli, A.A., and Lowe, S.W. (2002). Apoptosis: a link between cancer genetics and chemotherapy. Cell *108*, 153–164. https://doi.org/10.1016/s0092-8674(02)00625-6.
13. Hengartner, M.O., and Horvitz, H.R. (1994). Programmed cell death in Caenorhabditis elegans. Curr. Opin. Genet. Dev. *4*, 581–586. https://doi.org/10.1016/0959-437x(94)90076-f.
14. Ellis, H.M., and Horvitz, H.R. (1986). Genetic control of programmed cell death in the nematode C. elegans. Cell *44*, 817–829. https://doi.org/10.1016/0092-8674(86)90004-8.
15. McIlwain, D.R., Berger, T., and Mak, T.W. (2013). Caspase functions in cell death and disease. Cold Spring Harb. Perspect. Biol. *5*, a008656. https://doi.org/10.1101/cshperspect.a008656.
16. Yuan, J., Shaham, S., Ledoux, S., Ellis, H.M., and Horvitz, H.R. (1993). The C. elegans cell death gene ced-3 encodes a protein similar to mammalian interleukin-1 beta-converting enzyme. Cell *75*, 641–652. https://doi.org/10.1016/0092-8674(93)90485-9.
17. Van Opdenbosch, N., and Lamkanfi, M. (2019). Caspases in Cell Death, Inflammation, and Disease. Immunity *50*, 1352–1364. https://doi.org/10.1016/j.immuni.2019.05.020.
18. Nakajima, Y.I., and Kuranaga, E. (2017). Caspase-dependent non-apoptotic processes in development. Cell Death Differ. *24*, 1422–1430. https://doi.org/10.1038/cdd.2017.36.
19. Julien, O., and Wells, J.A. (2017). Caspases and their substrates. Cell Death Differ. *24*, 1380–1389. https://doi.org/10.1038/cdd.2017.44.
20. Chen, Y.Z., Mapes, J., Lee, E.S., Skeen-Gaar, R.R., and Xue, D. (2013). Caspase-mediated activation of Caenorhabditis elegans CED-8 promotes apoptosis and phosphatidylserine externalization. Nat. Commun. *4*, 2726. https://doi.org/10.1038/ncomms3726.
21. Meng, L., Mulcahy, B., Cook, S.J., Neubauer, M., Wan, A., Jin, Y., and Yan, D. (2015). The Cell Death Pathway Regulates Synapse Elimination through Cleavage of Gelsolin in Caenorhabditis elegans Neurons. Cell Rep. *11*, 1737–1748. https://doi.org/10.1016/j.celrep.2015.05.031.
22. Kutscher, L.M., and Shaham, S. (2017). Non-apoptotic cell death in animal development. Cell Death Differ. *24*, 1326–1336. https://doi.org/10.1038/cdd.2017.20.
23. Xue, D., Shaham, S., and Horvitz, H.R. (1996). The Caenorhabditis elegans cell-death protein CED-3 is a cysteine protease with substrate specificities similar to those of the human CPP32 protease. Genes Dev. *10*, 1073–1083. https://doi.org/10.1101/gad.10.9.1073.
24. Ghose, P., and Shaham, S. (2020). Cell death in animal development. Development *147*, dev191882. https://doi.org/10.1242/dev.191882.
25. Ghose, P., Rashid, A., Insley, P., Trivedi, M., Shah, P., Singhal, A., Lu, Y., Bao, Z., and Shaham, S. (2018). EFF-1 fusogen promotes phagosome sealing during cell process clearance in Caenorhabditis elegans. Nat. Cell Biol. *20*, 393–399. https://doi.org/10.1038/s41556-018-0068-5.
26. Datar, A., Ameeramja, J., Bhat, A., Srivastava, R., Mishra, A., Bernal, R., Prost, J., Callan-Jones, A., and Pullarkat, P.A. (2019). The Roles of Microtubules and Membrane Tension in Axonal Beading, Retraction, and Atrophy. Biophys. J. *117*, 880–891. https://doi.org/10.1016/j.bpj.2019.07.046.
27. Furusawa, K., and Emoto, K. (2021). Spatiotemporal regulation of developmental neurite pruning: Molecular and cellular insights from Drosophila models. Neurosci. Res. *167*, 54–63. https://doi.org/10.1016/j.neures.2020.11.010.
28. Low, L.K., and Cheng, H.J. (2006). Axon pruning: an essential step underlying the developmental plasticity of neuronal connections. Philos. Trans. R. Soc. Lond. B Biol. Sci. *361*, 1531–1544. https://doi.org/10.1098/rstb.2006.1883.
29. Ghose, P., and Wehman, A.M. (2021). The developmental and physiological roles of phagocytosis in Caenorhabditis elegans. Curr. Top. Dev. Biol. *144*, 409–432. https://doi.org/10.1016/bs.ctdb.2020.09.001.
30. Patel, N., Thierry-Mieg, D., and Mancillas, J.R. (1993). Cloning by insertional mutagenesis of a cDNA encoding Caenorhabditis elegans kinesin heavy chain. Proc. Natl. Acad. Sci. USA *90*, 9181–9185. https://doi.org/10.1073/pnas.90.19.9181.
31. Pilling, A.D., Horiuchi, D., Lively, C.M., and Saxton, W.M. (2006). Kinesin-1 and Dynein are the primary motors for fast transport of mitochondria in Drosophila motor axons. Mol. Biol. Cell *17*, 2057–2068. https://doi.org/10.1091/mbc.e05-06-0526.
32. Bock, F.J., and Tait, S.W.G. (2020). Mitochondria as multifaceted regulators of cell death. Nat. Rev. Mol. Cell Biol. *21*, 85–100. https://doi.org/10.1038/s41580-019-0173-8.
33. Rawson, R.L., Yam, L., Weimer, R.M., Bend, E.G., Hartwieg, E., Horvitz, H.R., Clark, S.G., and Jorgensen, E.M. (2014). Axons degenerate in the absence of mitochondria in C. elegans. Curr. Biol. *24*, 760–765. https://doi.org/10.1016/j.cub.2014.02.025.
34. Maurer, C.W., Chiorazzi, M., and Shaham, S. (2007). Timing of the onset of a developmental cell death is controlled by transcriptional induction of the C. elegans ced-3 caspase-encoding gene. Development *134*, 1357–1368. https://doi.org/10.1242/dev.02818.
35. Zhang, J., Wang, X., Cui, W., Wang, W., Zhang, H., Liu, L., Zhang, Z., Li, Z., Ying, G., Zhang, N., and Li, B. (2013). Visualization of caspase-3-like activity in cells using a genetically encoded fluorescent biosensor activated by protein cleavage. Nat. Commun. *4*, 2157. https://doi.org/10.1038/ncomms3157.
36. Wu, Y., Ding, C., Sharif, B., Weinreb, A., Swaim, G., Hao, H., Yogev, S., Watanabe, S., and Hammarlund, M. (2024). Polarized localization of kinesin-1 and RIC-7 drives axonal mitochondria anterograde transport. J. Cell Biol. *223*, e202305105. https://doi.org/10.1083/jcb.202305105.
37. Otsuka, A.J., Jeyaprakash, A., García-Añoveros, J., Tang, L.Z., Fisk, G., Hartshorne, T., Franco, R., and Born, T. (1991). The C. elegans unc-104 gene encodes a putative kinesin heavy chain-like protein. Neuron *6*, 113–122. https://doi.org/10.1016/0896-6273(91)90126-k.
38. Felkai, S., Ewbank, J.J., Lemieux, J., Labbé, J.C., Brown, G.G., and Hekimi, S. (1999). CLK-1 controls respiration, behavior and aging in the nematode Caenorhabditis elegans. EMBO J. *18*, 1783–1792. https://doi.org/10.1093/emboj/18.7.1783.
39. Xu, S., and Chisholm, A.D. (2014). C. elegans epidermal wounding induces a mitochondrial ROS burst that promotes wound repair. Dev. Cell *31*, 48–60. https://doi.org/10.1016/j.devcel.2014.08.002.
40. Tian, L., Hires, S.A., Mao, T., Huber, D., Chiappe, M.E., Chalasani, S.H., Petreanu, L., Akerboom, J., McKinney, S.A., Schreiter, E.R., et al. (2009). Imaging neural activity in worms, flies and mice with improved GCaMP calcium indicators. Nat. Methods *6*, 875–881. https://doi.org/10.1038/nmeth.1398.
41. Srayko, M., Kaya, A., Stamford, J., and Hyman, A.A. (2005). Identification and characterization of factors required for microtubule growth and nucleation in the early C. elegans embryo. Dev. Cell *9*, 223–236. https://doi.org/10.1016/j.devcel.2005.07.003.

42. Han, S.M., Baig, H.S., and Hammarlund, M. (2016). Mitochondria Localize to Injured Axons to Support Regeneration. Neuron *92*, 1308–1323. https://doi.org/10.1016/j.neuron.2016.11.025.

43. Rosenkranz, S.C., Shaposhnykov, A.A., Träger, S., Engler, J.B., Witte, M. E., Roth, V., Vieira, V., Paauw, N., Bauer, S., Schwencke-Westphal, C., et al. (2021). Enhancing mitochondrial activity in neurons protects against neurodegeneration in a mouse model of multiple sclerosis. eLife *10*, e61798. https://doi.org/10.7554/eLife.61798.

44. Zaglia, T., Campo, A., Moro, N., Di Mauro, V., Borile, G., Menabò, R., Antonucci, S., Poli, L., Campesan, M., Carullo, P., et al. (2025). Enhancement of mitochondrial calcium uptake is cardioprotective against maladaptive hypertrophy by retrograde signaling uptuning Akt. Proc. Natl. Acad. Sci. USA *122*, e2402639122. https://doi.org/10.1073/pnas.2402639122.

45. Angelova, P.R., Vinogradova, D., Neganova, M.E., Serkova, T.P., Sokolov, V.V., Bachurin, S.O., Shevtsova, E.F., and Abramov, A.Y. (2019). Pharmacological Sequestration of Mitochondrial Calcium Uptake Protects Neurons Against Glutamate Excitotoxicity. Mol. Neurobiol. *56*, 2244–2255. https://doi.org/10.1007/s12035-018-1204-8.

46. Spiess, K.L., Geden, M.J., Romero, S.E., Hollville, E., Hammond, E.S., Patterson, R.L., Girardi, Q.B., and Deshmukh, M. (2025). Apoptosis signaling is activated as a transient pulse in neurons. Cell Death Differ. *32*, 521–529. https://doi.org/10.1038/s41418-024-01403-5.

47. Sure, G.R., Chatterjee, A., Mishra, N., Sabharwal, V., Devireddy, S., Awasthi, A., Mohan, S., and Koushika, S.P. (2018). UNC-16/JIP3 and UNC-76/FEZ1 limit the density of mitochondria in C. elegans neurons by maintaining the balance of anterograde and retrograde mitochondrial transport. Sci. Rep. *8*, 8938. https://doi.org/10.1038/s41598-018-27211-9.

48. Hall, D.H., and Hedgecock, E.M. (1991). Kinesin-related gene unc-104 is required for axonal transport of synaptic vesicles in C. elegans. Cell *65*, 837–847. https://doi.org/10.1016/0092-8674(91)90391-b.

49. Lo, K.Y., Kuzmin, A., Unger, S.M., Petersen, J.D., and Silverman, M.A. (2011). KIF1A is the primary anterograde motor protein required for the axonal transport of dense-core vesicles in cultured hippocampal neurons. Neurosci. Lett. *491*, 168–173. https://doi.org/10.1016/j.neulet.2011.01.018.

50. Fuchs, F., and Westermann, B. (2005). Role of Unc104/KIF1-related motor proteins in mitochondrial transport in Neurospora crassa. Mol. Biol. Cell *16*, 153–161. https://doi.org/10.1091/mbc.e04-05-0413.

51. Tanaka, K., Sugiura, Y., Ichishita, R., Mihara, K., and Oka, T. (2011). KLP6: a newly identified kinesin that regulates the morphology and transport of mitochondria in neuronal cells. J. Cell Sci. *124*, 2457–2465. https://doi.org/10.1242/jcs.086470.

52. Nangaku, M., Sato-Yoshitake, R., Okada, Y., Noda, Y., Takemura, R., Yamazaki, H., and Hirokawa, N. (1994). KIF1B, a novel microtubule plus end-directed monomeric motor protein for transport of mitochondria. Cell *79*, 1209–1220. https://doi.org/10.1016/0092-8674(94)90012-4.

53. Hummel, J.J.A., and Hoogenraad, C.C. (2021). Specific KIF1A-adaptor interactions control selective cargo recognition. J. Cell Biol. *220*, e202105011. https://doi.org/10.1083/jcb.202105011.

54. Hirokawa, N., Noda, Y., Tanaka, Y., and Niwa, S. (2009). Kinesin superfamily motor proteins and intracellular transport. Nat. Rev. Mol. Cell Biol. *10*, 682–696. https://doi.org/10.1038/nrm2774.

55. Schnapp, B.J. (2003). Trafficking of signaling modules by kinesin motors. J. Cell Sci. *116*, 2125–2135. https://doi.org/10.1242/jcs.00488.

56. Mallik, R., and Gross, S.P. (2004). Molecular motors: strategies to get along. Curr. Biol. *14*, R971–R982. https://doi.org/10.1016/j.cub.2004.10.046.

57. Klopfenstein, D.R., and Vale, R.D. (2004). The lipid binding pleckstrin homology domain in UNC-104 kinesin is necessary for synaptic vesicle transport in Caenorhabditis elegans. Mol. Biol. Cell *15*, 3729–3739. https://doi.org/10.1091/mbc.e04-04-0326.

58. Kumar, J., Choudhary, B.C., Metpally, R., Zheng, Q., Nonet, M.L., Ramanathan, S., Klopfenstein, D.R., and Koushika, S.P. (2010). The Caenorhabditis elegans Kinesin-3 motor UNC-104/KIF1A is degraded upon loss of specific binding to cargo. PLoS Genet. *6*, e1001200. https://doi.org/10.1371/journal.pgen.1001200.

59. Labrousse, A.M., Zappaterra, M.D., Rube, D.A., and van der Bliek, A.M. (1999). C. elegans dynamin-related protein DRP-1 controls severing of the mitochondrial outer membrane. Mol. Cell *4*, 815–826. https://doi.org/10.1016/s1097-2765(00)80391-3.

60. Moujalled, D., Strasser, A., and Liddell, J.R. (2021). Molecular mechanisms of cell death in neurological diseases. Cell Death Differ. *28*, 2029–2044. https://doi.org/10.1038/s41418-021-00814-y.

61. Llobet Rosell, A., and Neukomm, L.J. (2019). Axon death signalling in Wallerian degeneration among species and in disease. Open Biol. *9*, 190118. https://doi.org/10.1098/rsob.190118.

62. Koppers, M., and Farías, G.G. (2021). Organelle distribution in neurons: Logistics behind polarized transport. Curr. Opin. Cell Biol. *71*, 46–54. https://doi.org/10.1016/j.ceb.2021.02.004.

63. Hollenbeck, P.J., and Saxton, W.M. (2005). The axonal transport of mitochondria. J. Cell Sci. *118*, 5411–5419. https://doi.org/10.1242/jcs.02745.

64. Ng, R., Wu, S.T., and Su, C.Y. (2020). Neuronal Compartmentalization: A Means to Integrate Sensory Input at the Earliest Stage of Information Processing? BioEssays *42*, e2000026. https://doi.org/10.1002/bies.202000026.

65. Brenner, S. (1974). The genetics of Caenorhabditis elegans. Genetics *77*, 71–94. https://doi.org/10.1093/genetics/77.1.71.

66. Mello, C.C., Kramer, J.M., Stinchcomb, D., and Ambros, V. (1991). Efficient gene transfer in C.elegans: extrachromosomal maintenance and integration of transforming sequences. EMBO J. *10*, 3959–3970. https://doi.org/10.1002/j.1460-2075.1991.tb04966.x.

67. Dokshin, G.A., Ghanta, K.S., Piscopo, K.M., and Mello, C.C. (2018). Robust Genome Editing with Short Single-Stranded and Long, Partially Single-Stranded DNA Donors in Caenorhabditis elegans. Genetics *210*, 781–787. https://doi.org/10.1534/genetics.118.301532.

68. Wicks, S.R., Yeh, R.T., Gish, W.R., Waterston, R.H., and Plasterk, R.H. (2001). Rapid gene mapping in Caenorhabditis elegans using a high density polymorphism map. Nat. Genet. *28*, 160–164. https://doi.org/10.1038/88878.

69. Wu, Y., Wawrzusin, P., Senseney, J., Fischer, R.S., Christensen, R., Santella, A., York, A.G., Winter, P.W., Waterman, C.M., Bao, Z., et al. (2013). Spatially isotropic four-dimensional imaging with dual-view plane illumination microscopy. Nat. Biotechnol. *31*, 1032–1038. https://doi.org/10.1038/nbt.2713.

70. Edelstein, A., Amodaj, N., Hoover, K., Vale, R., and Stuurman, N. (2010). Computer control of microscopes using μManager. Curr. Protoc. Mol. Biol. *92*. 14.20.1–14.20.17. https://doi.org/10.1002/0471142727.mb1420s92.

71. Dey, S., and Ghosh-Roy, A. (2021). In vivo Assessment of Microtubule Dynamics and Orientation in Caenorhabditis elegans Neurons. J. Vis. Exp. *177*, 10–3791. https://doi.org/10.3791/62744.

STAR★METHODS

KEY RESOURCES TABLE

REAGENT or RESOURCE	SOURCE	IDENTIFIER
Chemicals, peptides, and recombinant proteins		
trioxsalen	Sigma	Cat#T2137
sodium azide	VWR	Cat#BDH7465-2
ethyl methanesulfonate	Sigma	Cat#M0880
Experimental models: Organisms/strains		
C. elegans: Strain FX03150: *miro-3(tm3150)/I*	NBRP	WormBase: *miro-3*
C. elegans: Strain CB1265: *unc-104(e1265)/II*	CGC	WormBase: *unc-104*
C. elegans: Strain FF41: *unc-116(e2310)/III*	CGC	WormBase: *unc-116*
C. elegans: Strain MT2547: *ced-4(n1162)/III*	CGC	WormBase: *ced-4*
C. elegans: Strain MQ130: *clk-1(qm30)/III*	CGC	WormBase: *clk-1*
C. elegans: Strain MT1522: *ced-3(n717)/IV*	CGC	WormBase: *ced-3*
C. elegans: Strain MT7004 *ced-3(n2427)/IV*	Shaham Lab	WormBase: *ced-3*
C. elegans: Strain CZ19982: *mcu-1(ju1154)/IV*	CGC	WormBase: *mcu-1*
C. elegans: Strain FX01966: *miro-1(tm1966)/IV*	NBRP	WormBase: *miro-1*
C. elegans: Strain MT6924: *ric-7(n2567)/V*	CGC	WormBase: *ric-7*
C. elegans: Strain NM1489: *dhc-1(js319)X*	Kaushika Lab	WormBase: *dhc-1*
C. elegans: Strain *miro-2(tm2933)/X*	CGC	WormBase: *miro-2*
C. elegans: Strain *unc-116(ns827)/III*	This Paper	N/A
C. elegans: Strain TSC6: *unc-116(e2310)/III; nsIs435*; *nsIs435=aff-1*p::myrGFP	This Paper	N/A
C. elegans: Strain TSC16: *ced-3(n717)/IV; nsIs435; mccEx006*; *mccEx006*=pPG245; *nsIs435=aff-1*p::myrGFP	This Paper	N/A
C. elegans: Strain TSC17: *ced-3(n717)/IV; nsIs435; mccEx007*; *mccEx007*=pPG245; *nsIs435=aff-1*p::myrGFP	This Paper	N/A
C. elegans: Strain TSC32: *unc-116(ns827)/III; mccEx019*; *mccEx019*=pPG246; *nsIs435=aff-1*p::myrGFP	This Paper	N/A
C. elegans: Strain TSC33: *unc-116(ns827/)/III; mccEx020*; *mccEx020*=pPG246; *nsIs435=aff-1*p::myrGFP	This Paper	N/A
C. elegans: Strain TSC40: *unc-116(ns827/III); nsIs686; mccIs005*; *mccIs005*=pPG112; *nsIs686=aff-1*p::mKate2	This Paper	N/A
C. elegans: Strain TSC66: *ced-3(n717)/IV; nsIs686; mccIs005*; *mccIs005*=pPG112; *nsIs686=aff-1*p::mKate2	This Paper	N/A
C. elegans: Strain TSC74: *unc-104(e1265)/II; ced-3(n2427); nsIs435*; *nsIs435=aff-1*p::myrGFP	This Paper	N/A
C. elegans: Strain TSC89: *unc-104(e1265)/II; nsIs435*; *nsIs435=aff-1*p::myrGFP	This Paper	N/A
C. elegans: Strain TSC90: *trak-1(tm1572)/I; ced-3(n2427); nsIs435*; *nsIs435=aff-1*p::myrGFP	This Paper	N/A
C. elegans: Strain TSC91: *trak-1(tm1572)/I; nsIs435*; *nsIs435=aff-1*p::myrGFP	This Paper	N/A
C. elegans: Strain TSC96: *unc-116(ns827)/III;ced-3(n2427);nsIs435*; *nsIs435=aff-1*p::myrGFP	This Paper	N/A
C. elegans: Strain TSC98: *unc-116(ns827)/III; nsIs435; mccEx047*; *mccEx047*=pPG174; *nsIs435=aff-1*p::myrGFP	This Paper	N/A
C. elegans: Strain TSC99: *unc-116(ns827)/III; nsIs435; mccEx048*; *mccEx048*=pPG174; *nsIs435=aff-1*p::myrGFP	This Paper	N/A
C. elegans: Strain TSC100: *unc-116(ns827)/III; nsIs435; mccEx049*; *mccEx049*=pPG174; *nsIs435=aff-1*p::myrGFP	This Paper	N/A
C. elegans: Strain TSC105: *unc-104(e1265)/II; ced-3(n2427)/IV; nsIs435; mccEx053*; *mccEx053*=pPG294; *nsIs435=aff-1*p::myrGFP	This Paper	N/A

(*Continued on next page*)

Continued

REAGENT or RESOURCE	SOURCE	IDENTIFIER
C. elegans: Strain TSC106: *unc-104(e1265); ced-3(n2427); nsIs435; mccEx054*; *mccEx054*=pPG294; *nsIs435=aff-1*p::myrGFP	This Paper	N/A
C. elegans: Strain TSC107: *unc-104(e1265)/II; ced-3(n2427)/IV; nsIs435; mccEx055*; *mccEx055*=pPG294; *nsIs435=aff-1*p::myrGFP	This Paper	N/A
C. elegans: Strain TSC260: *ced-3(n717)/IV; nsIs532*; *nsIs532*=pPG114	This Paper	N/A
C. elegans: Strain TSC261; *ced-3(n717)/IV; nsIs560 nsIs560*=pPG113	This Paper	N/A
C. elegans: Strain TSC264; *unc-116(ns827)/III; ced-3(n717)/IV; nsIs686; mccIs005*; *mccIs005*=pPG112; *nsIs686=aff-1*p::mKate2	This Paper	N/A
C. elegans: Strain TSC277: *ced-3(n2427)/IV; dhc-1(js319)/X; nsIs435*; *nsIs435=aff-1*p::myrGFP	This Paper	N/A
C. elegans: Strain TSC304: *unc-104(e1265)/II; ced-3(n2427)/IV; nsIs435; mccEx156*; *mccEx156*=pPG331; *nsIs435=aff-1*p::myrGFP	This Paper	N/A
C. elegans: Strain TSC305:*unc-104(e1265)/II; ced-3(n2427)/IV; nsIs435; mccEx157*; *mccEx157*=pPG331; *nsIs435=aff-1*p::myrGFP	This Paper	N/A
C. elegans: Strain TSC306; *unc-104(e1265)/II; ced-3(n2427)/IV; nsIs435; mccEx158*; *mccEx158*=pPG331; *nsIs435=aff-1*p::myrGFP	This Paper	N/A
C. elegans: Strain TSC386: *unc-116(ns827)/III; ced-3(n717)/IV; nsIs686; mccIs005; mcc27*; *mcc27*=Small deletion few nucleotides upstream PAM site; *mccIs005*=pPG112; *nsIs686=aff-1*p::mKate2	This Paper	N/A
C. elegans: Strain TSC404: *ced-3(n717)/IV; mcc28*; *mcc28*=GFP inserted just before stop codon (C terminus)	This Paper	N/A
C. elegans: Strain TSC405: *ced-3(n717)/IV; mcc28; mccIs094*; *mcc28*=GFP inserted just before stop codon (C terminus); *mccIs094=mccEx207=aff-1p(small)::TSC myrmCherry*	This Paper	N/A
C. elegans: Strain TSC407:*ced-4(n1162)III; nsIs686; mccIs015*; *mccIs015*=pPG274; *nsIs686=aff-1*p::mKate2	This Paper	N/A
C. elegans: Strain TSC409:*clk-1(qm30)III; ced-3(n2427)/IV; nsIs435*; *nsIs435=aff-1*p::myrGFP	This Paper	N/A
C. elegans: Strain TSC459: *unc-116(mcc33)/III*; *mcc33*=[UNC-116::GFP] N2; CRISPR mutant, GFP insertion after UNC-116	This Paper	N/A
C. elegans: Strain TSC472: *clk-1(qm30)/III*; *nsIs435;nsIs435=aff-1*p::myrGFP	This Paper	N/A
C. elegans: Strain TSC489: *N2; mcc33; mccEx207*; *mcc33*=[UNC-116::GFP] N2; CRISPR mutant, GFP insertion after UNC-116; *mccEx207=aff-1*p::myrmCherry	This Paper	N/A
C. elegans: Strain TSC514: *ced-3(n717)/IV; mccIs002; mccIs050*; *mccIs002*=pPG112; *mccIs050*=pPG401	This Paper	N/A
C. elegans: Strain TSC521: *dhc-1(js319)/X; nsIs435*; *nsIs435=aff-1*p::myrGFP	This Paper	N/A
C. elegans: Strain TSC522:*mcu-1(ju1154)/IV; nsIs435*; *nsIs435=aff-1*p::myrGFP	This Paper	N/A
C. elegans: Strain TSC577: *N2; mcc28/II; mccIs094*; *mcc28*=UNC-104::GFP inserted just before stop codon (C terminus); *mccIs094=aff-1*p::myrmCherry	This Paper	N/A
C. elegans: Strain TSC580: *ced-3(n717)/IV; mcc28/II; mccIs100*; *mcc28*=UNC-104::GFP inserted just before stop codon (C terminus); *mccIs100=aff-1*p::myrmCherry	This Paper	N/A
C. elegans: Strain TSC581: *N2; mcc33/III; mccIs094*; *mcc33*=[UNC-116::GFP] N2; CRISPR mutant, GFP insertion after UNC-116; *mccIs094=aff-1*p::myrmCherry	This Paper	N/A
C. elegans: Strain TSC582: *N2; mcc33/III; mccIs100*; *mcc33*=[UNC-116::GFP] N2; CRISPR mutant, GFP insertion after UNC-116; *mccIs100=aff-*1p::myrmCherry	This Paper	N/A
C. elegans: Strain TSC681: *ced-(n717)/IV; nsIs560*; *nsIs560*=pPG113	This Paper	N/A
C. elegans: Strain TSC682: *ced-(n717)/IV; mcu-1(ju1154)/IV; nsIs560*; *nsIs560*=pPG113	This Paper	N/A
C. elegans: Strain TSC683: *ced-(n717)/IV; unc-104(e1265)/II; nsIs560*; *nsIs560*=pPG113	This Paper	N/A

(*Continued on next page*)

Continued

REAGENT or RESOURCE	SOURCE	IDENTIFIER
C. elegans: Strain TSC685: *mcu-1(syb6842)/IV; ced-3(n2427)/IV; nsIs435*; *mccEx276;mccEx276*=pPG445; *nsIs435=aff-1*p::myrGFP	This Paper	N/A
C. elegans: Strain TSC686: *mcu-1(syb6842)/IV; ced-3(n2427)/IV; nsIs435*; *mccEx277;mccEx277*=pPG445; *nsIs435=aff-1*p::myrGFP	This Paper	N/A
C. elegans: Strain TSC688: *mcu-1(syb6842)/IV; ced-3(n2427)/IV; nsIs435; mccEx279*; *mccEx279*=pPG445; *nsIs435=aff-1*p::myrGFP	This Paper	N/A
C. elegans: Strain TSC693: *ced-3(n717)/IV; unc-104(e1265)/II; nsIs686; mccIs005*; *mccIs005*=pPG112; *nsIs686=aff-1*p::mKate2	This Paper	N/A
C. elegans: Strain OS8095: *ced-3(n717)/IV; nsIs435*; *nsIs435=aff-1*p::myrGFP	This Paper	N/A
C. elegans: Strain OS9235:*ced-3(n2427)/IV; nsIs435*; *nsIs435=aff-1*p::myrGFP	This Paper	N/A
C. elegans: Strain OS9985: *N2; nsIs532*; *nsIs532*=pPG114	This Paper	N/A
C. elegans: Strain OS10204: *N2; nsIs560*; *nsIs560*=pPG113	This Paper	N/A
C. elegans: Strain OS11918:*unc-116(ns827)/III; nsIs435*; *nsIs435=aff-1*p::myrGFP	This Paper	N/A
C. elegans: Strain PHX6842: *mcu-1(syb6842)/IV; ced-3(n2427)/IV*	This Paper	N/A
Oligonucleotides		
crRNA for UNC-104 CRISPR GFP- 5'-GCAATTGAAGATGATGATGT-3'.	This Paper	N/A
crRNA for UNC-116 CRISPR GFP 5'- GTTAAATTTGATAATACGGT-3'.	This Paper	N/A
Primers for Recombinant DNA, see Table S1	This Paper	N/A
Recombinant DNA		
pPG294; TSCp::unc-104 cDNA (cell specific rescue)	This Paper	N/A
pPG331; TSCp::unc-104GFP_tomm7 (mito rescue)	This Paper	N/A
pPG445; TSCp::mcu-1 cDNA (cell specific rescue)	This Paper	N/A
pPG245unc-116p::mKate2 (expression)	This Paper	N/A
pPG246; TSCp::unc-116 cDNA (cell specific rescue)	This Paper	N/A
pPG401; TSCp::UNC-104::mCherry	This Paper	N/A
pPG274; TSCp::EBP-2::GFP	This Paper	N/A
pPG174; TSCp::unc116GFP_tomm7	This Paper	N/A
pPG115; TSCp::GCaMP5a_SL2_myrmcherry	This Paper	N/A
pPG113; TSCp::GFP::C3Ai_SL2::myrmCherry	This Paper	N/A
pPG112; TSCp::mitoGFP	This Paper	N/A
pPG114; TSCp::mitoGFP_SL2_myrmcherry	This Paper	N/A
Software and algorithms		
ImageJ	NIH	https://imagej.nih.gov/ij/
Prism 10	Graphpad	https://www.graphpad.com/
NIS Elements	NIkon	https://www.microscope.healthcare.nikon.com/products/software/nis-elements

EXPERIMENTAL MODEL AND STUDY PARTICIPANT DETAILS

C. elegans culture

C. elegans strains were cultured per standard methods and were grown at 20°C.[65] Wild-type animals were of the Bristol N2 subspecies. For most tail-spike cell (TSC) experiments, one of three integrated reporters were used: *nsIs435*, *nsIs431*, or *nsIs686*. Integration of extrachromosomal arrays was performed using UV and trioxsalen (Sigma T2137). Larvae were scored at 20°C at the L1 stage. All wild-type, mutant and transgenic strains used are listed in key resources table.

METHOD DETAILS

Germline transformation and rescue experiments

Germline transformation was carried out as previously described.[66] All plasmids were injected at between 1 and 20ng/μL. pBSK was used to adjust the DNA concentration of injection mixtures if necessary. All rescue experiments were done with *myo-2*p::GFP as a co-injection marker along with *cdh-3*p::mCherry to label the TSC.

Primers and plasmid construction

Plasmids were generated by either Gibson Cloning or restriction digest. Primer sequences and information on the construction of plasmids used in this study are provided in Table S1. The full length or fragment of the *aff-1* promoter was used in generating constructs for TSC expression.

CRISPR-Cas9 genome editing

To generate TSC404, GFP was introduced to the C-terminus of *unc-104* via CRISPR-Cas9 using the crRNA- 5'-GCAATTGAAGATGA TGATGT-3'. To generate TSC459, GFP was introduced to the C-terminus of *unc-116* via CRISPR/Cas9 using the crRNA 5'- GTT AAATTTGATAATACGGT-3'. Mutants were generated using a co-injection strategy.[67] Guide crRNA, repair single-stranded DNA oligos, tracrRNA, and buffers were ordered from IDT. The strain PHX6842, *mcu-1(syb6842);ced-3(n2427);nsIs435*, was made by deleting base pairs 468 to 1364 from the gene *mcu-1* in the background of *ced-3(n2427);nsIs435* and was generated by Suny Biotech (Suzhou, Jiangsu, China 215028).

Scoring of TSC/CCE defects

TSC death was scored at the L1 stage. Animals were synchronized allowing gravid hermaphrodites to lay eggs overnight, washing off larvae the next day and waiting 5 hours for hatched L1s. L1s synchronized were then mounted on slides on 2% agarose-water pads, anaesthetized in 10 mM sodium azide and examined on a wide-field Axioscope A1 (Zeiss) at 40X magnification (NA 1.3). The TSC was identified by fluorescence (from reporter transgenes) as well as by its location and morphology.

Mutagenesis and mutant identification

nsIs435 animals were mutagenized using 75 mM ethyl methanesulfonate (M0880, Sigma) for 4 hours at 20°C. Approximately 27,000 F2 progeny were screened for TSC persistence on a Zeiss Axio-Scope A1 at 40X. *unc-116(ns827)* was identified from analysis of SNP-mapping,[68] Whole Genome Sequencing data, fosmid rescue and candidate gene analysis.

Microscopy and image processing

Images were collected on a Nikon TI2-E Inverted microscope using a CFI60 Plan Apochromat Lambda 60x Oil Immersion Objective Lens, N.A. 1.4 (Nikon) and a Yokogawa W1 Dual Cam Spinning Disk Confocal. Images were acquired using NIS-Elements Advanced Research Package. For still embryo imaging, embryos were anesthetized using 0.5M sodium azide. Larvae were paralyzed with 10mM sodium azide.

Light sheet imaging was performed using a customized ASI diSPIM[69] equipped with symmetric 40X Nikon CFI APO NIR objectives and imaged onto Hamamatsu Orca Fusion (C14440-20UP) cameras equipped with Hamamatsu W-View Gemini channel splitters for simultaneous two-color imaging. Imaging was performed with a single view 1 micron z-spacing and volumes were acquired every 3 minutes using the diSPIM control plug-in for Micro-Manager 1.4[70] and a uniform background subtraction of 100 counts was applied using ImageJ.

EBP-2 imaging was done on *ced-3(n717)* mutant L1 larvae following previously published protocol[71] on the Nikon TI2-E Inverted microscope above. Kymographs were generated using ImageJ.

QUANTIFICATION AND STATISTICAL ANALYSES

Descriptions of statistical tests and group sizes are provided in figure legends.

Quantification of mitochondria

Length of TSC process and number of mitochondria in the TSC process was counted using ImageJ using analyze particle tool. Mitochondria number/TSC process length was calculated in Excel, and these values were input in GraphPad to generate graph.

Quantification of Fluorescence Intensity

Sum intensity projections of fluorescent reporters in relevant cell regions were generated by following TSC membrane signal in ImageJ software, and GFP intensity was measured. Corrected Total Cell Fluorescence (CTCF) was calculated using Microsoft Excel and graphed using GraphPad Prism. Statistical analysis: unpaired two-tailed t-test for comparison between wild-type and mutant animals.

Statistics and reproducibility

The sample sizes and statistical tests were selected based on previous studies with similar methodologies. Sample sizes were not determined using statistical methods. All experiments were repeated at least two to three times, as indicated, giving similar results. Independent transgenic lines were treated as independent experiments. Quantification of TSC persistence was done using an unpaired two-tailed *t*-test (GraphPad). For all Figures, mean ± standard error of the mean (s.e.m.) is represented.